AFRL-RX-WP-JA-2015-0202

ACCELERATED EXPLORATION OF MULTI-PRINCIPAL ELEMENT ALLOYS FOR STRUCTURAL APPLICATIONS (POSTPRINT)

O. N. Senkov, J. D.Miller, D. B. Miracle, and C.Woodward
AFRL/RXCM

MAY 2015
Interim Report

AIR FORCE RESEARCH LABORATORY
MATERIALS AND MANUFACTURING DIRECTORATE
WRIGHT-PATTERSON AIR FORCE BASE OH 45433-7750
AIR FORCE MATERIEL COMMAND
UNITED STATES AIR FORCE

NOTICE AND SIGNATURE PAGE

Using Government drawings, specifications, or other data included in this document for any purpose other than Government procurement does not in any way obligate the U.S. Government. The fact that the Government formulated or supplied the drawings, specifications, or other data does not license the holder or any other person or corporation; or convey any rights or permission to manufacture, use, or sell any patented invention that may relate to them.

Qualified requestors may obtain copies of this report from the Defense Technical Information Center (DTIC) (http://www.dtic.mil).

AFRL-RX-WP-JA-2015-0202 HAS BEEN REVIEWED AND IS APPROVED FOR PUBLICATION IN ACCORDANCE WITH ASSIGNED DISTRIBUTION STATEMENT.

//Signature//
_____
CHRISTOPHER F. WOODWARD, Project Engineer
Metals Branch
Structural Materials Division

//Signature//
_____
DANIEL J. EVANS, Chief
Metals Branch
Structural Materials Division

//Signature//
_____
ROBERT T. MARSHALL, Deputy Chief
Structural Materials Division
Materials And Manufacturing Directorate

This report is published in the interest of scientific and technical information exchange and its publication does not constitute the Government's approval or disapproval of its ideas or findings.

REPORT DOCUMENTATION PAGE

Form Approved
OMB No. 0704-0188

1. REPORT DATE *(DD-MM-YY)*	2. REPORT TYPE	3. DATES COVERED *(From - To)*
May 2015	Interim	19 March 2014 – 24 April 2015

4. TITLE AND SUBTITLE
ACCELERATED EXPLORATION OF MULTI-PRINCIPAL ELEMENT ALLOYS FOR STRUCTURAL APPLICATIONS (POSTPRINT)

5a. CONTRACT NUMBER
In-house

5b. GRANT NUMBER

5c. PROGRAM ELEMENT NUMBER
62102F

6. AUTHOR(S)
O. N. Senkov, J. D.Miller, D. B. Miracle, and C.Woodward

5d. PROJECT NUMBER
4349

5e. TASK NUMBER

5f. WORK UNIT NUMBER
X0W6

7. PERFORMING ORGANIZATION NAME(S) AND ADDRESS(ES)
Air Force Research Laboratory
Materials and Manufacturing Directorate
Wright-Patterson Air Force Base, Ohio 45433

8. PERFORMING ORGANIZATION REPORT NUMBER

9. SPONSORING/MONITORING AGENCY NAME(S) AND ADDRESS(ES)
Air Force Research Laboratory
Materials and Manufacturing Directorate
Wright-Patterson Air Force Base, OH 45433-7750
Air Force Materiel Command
United States Air Force

10. SPONSORING/MONITORING AGENCY ACRONYM(S)
AFRL/RXCM

11. SPONSORING/MONITORING AGENCY REPORT NUMBER(S)
AFRL-RX-WP-JA-2015-0202

12. DISTRIBUTION/AVAILABILITY STATEMENT
Distribution Statement A. Approved for public release: distribution unlimited.

13. SUPPLEMENTARY NOTES
Journal article published in *CALPHAD: Computer Coupling of Phase Diagrams and Thermochemistry* 50 (2015) 32-48. © 2015 Elsevier Ltd. The U.S. Government is joint author of the work and has the right to use, modify, reproduce, release, perform, display or disclose the work. This report contains color. The final publication is available at http://dx.doi.org/10.1016/j.calphad.2015.04.009.

14. ABSTRACT

A strategy for accelerated discovery and exploration of multi-principal element alloys was developed and used to identify new alloys within a design window of desired microstructures and properties. As an example, the strategy was applied to analyze thousands of 3- 4-, 5- and 6-component alloys at equia- tomic compositions of the alloying elements. Currently available thermodynamic databases were used to assess equilibrium phase diagrams for these alloys. The validity and reliability of the calculated phase diagrams were estimated based on the extent of experimental binary and ternary data used to build the respective thermodynamic databases. Alloys with specific characteristics, such as single-phase solid solution alloys with the use temperature above 1000°C, were identified using an automated analysis of the calculated phase diagrams. The density, elastic moduli and costs of these alloys were estimated using the rule of mixtures of pure elements and were used as additional criteria for alloy selection. This ap- proach allowed rapid, albeit preliminary, screening of many thousands of alloys and identification of promising candidate compositions, some of which are reported in this paper, for more time intensive experimental validations and assessments.

15. SUBJECT TERMS
alloy design, structural metals, high entropy alloys, multi-principal element alloys, calphad

16. SECURITY CLASSIFICATION OF:			17. LIMITATION OF ABSTRACT:	18. NUMBER OF PAGES	19a. NAME OF RESPONSIBLE PERSON (Monitor)
a. REPORT	b. ABSTRACT	c. THIS PAGE			Christopher F. Woodward
Unclassified	Unclassified	Unclassified	SAR	20	19b. TELEPHONE NUMBER *(Include Area Code)* (937) 255-9816

CALPHAD: Computer Coupling of Phase Diagrams and Thermochemistry 50 (2015) 32–48

Contents lists available at ScienceDirect

CALPHAD: Computer Coupling of Phase Diagrams and Thermochemistry

journal homepage: www.elsevier.com/locate/calphad

Accelerated exploration of multi-principal element alloys for structural applications

O.N. Senkov*, J.D. Miller, D.B. Miracle, C. Woodward

Air Force Research Laboratory, Materials and Manufacturing Directorate, Wright-Patterson AFB, OH 45433, USA

ARTICLE INFO

Article history:
Received 30 December 2014
Received in revised form
23 April 2015
Accepted 24 April 2015
Available online 27 April 2015

Keywords:
Alloy design
Structural metals
High entropy alloys
Multi-principal element alloys
Calphad

ABSTRACT

A strategy for accelerated discovery and exploration of multi principal element alloys was developed and used to identify new alloys within a design window of desired microstructures and properties. As an example, the strategy was applied to analyze thousands of 3 4 , 5 and 6 component alloys at equia tomic compositions of the alloying elements. Currently available thermodynamic databases were used to assess equilibrium phase diagrams for these alloys. The validity and reliability of the calculated phase diagrams were estimated based on the extent of experimental binary and ternary data used to build the respective thermodynamic databases. Alloys with specific characteristics, such as single phase solid solution alloys with the use temperature above 1000 °C, were identified using an automated analysis of the calculated phase diagrams. The density, elastic moduli and costs of these alloys were estimated using the rule of mixtures of pure elements and were used as additional criteria for alloy selection. This ap proach allowed rapid, albeit preliminary, screening of many thousands of alloys and identification of promising candidate compositions, some of which are reported in this paper, for more time intensive experimental validations and assessments.

1. Introduction

Materials with high strength, low density and acceptable da mage tolerance are in high demand for transportation and energy applications. Four alloy families are commonly used to meet the operating requirements in these applications. In order of increas ing application temperature, these are aluminum alloys, titanium alloys, iron alloys (steels and superalloys) and nickel based su peralloys. Alloy density generally increases with increasing use temperature. These alloys are each based on a single element with additional elements added to improve the balance of properties. The total concentration of secondary elements generally does not exceed 10 15%, but in superalloys it can be as high as 40% [1].

Ni based superalloys have been the material of choice for over 70 years in load bearing applications at the highest temperatures, especially in fracture critical components. Alloy density has in creased with the gradual evolutionary changes in alloy chemistry needed to improve the balance of properties (creep, strength, fa tigue) at higher temperatures [2]. Moreover, operating tempera tures of Ni based superalloys are now reaching theoretical limits, controlled by incipient melting at temperatures in the range of 1200 1300 °C. New materials with higher strength, higher oper ating temperatures and/or lower density are in high demand. Numerous concepts have been pursued in the past 50 years to surpass the balance of properties offered by these exceptional materials, but none have been successful in displacing superalloys [3].

Recently there has been a great deal of interest in a new alloy design strategy focused on multi principal element alloys (MPEA) where 3 6 elements are added at near equal atomic amounts [4 8]. This approach opens up a large composition space that has previously been unexplored and necessitates the use of a rapid screening technique to down select compositions that would give the best balance of properties. This assumes a priori knowledge of the best combinations of target phases and known metallurgical principles provide some guidance. One variant of this approach, known as High Entropy Alloys (HEAs), includes alloys containing 5 or more alloying elements at or near equiatomic amounts [4 6] and is focused on stabilizing a single solid solution phase. HEAs have interesting and unexpected microstructures and properties [4,5,7,9 11]. In spite of the compositional complexity, many HEAs have the tendency to form solid solution (SS) phases and the number of phases observed in these alloys is much less than the maximum predicted from the Gibbs phase rule [5,9,12 14]. For mation of a disordered SS phase in favor of an ordered IM phase in a HEA is explained [4,5,9 11] by higher entropy of mixing of al loying elements, ΔS_{mix}, in the multicomponent SS phase, relative to the entropy of formation, ΔS_f, of a competing IM compound. The difference between ΔS_{mix} and ΔS_f increases with an increase

* Corresponding author. Fax: +1 937 656 7292.

http://dx.doi.org/10.1016/j.calphad.2015.04.009
0364-5916/

in the number of the alloying elements and reaches its maximum at equiatomic compositions. Thus the reduction of the Gibbs free energy by the entropy term occurs with an increase in tempera ture more rapidly in SS than in IM phases. The HEA approach could be a powerful tool for producing new SS based high temperature structural alloys in an alloy composition space that has not been previously explored.

A brief survey of the literature shows significant alloy ex ploration in both face centered cubic (FCC) and body centered cubic (BCC) crystals. The FCC based HEAs contain Al, Co, Cr, Fe, Mn, Ni and Cu [14]. These can be considered an extension of austenitic stainless steels or superalloys, which have Fe, Cr and Ni as their major constituents but may also contain significant concentrations of other elements. Another group of HEAs reported in the litera ture is refractory containing HEAs [15,16]. The major phases in these alloys have body centered cubic (BCC) crystal structures and minor phases are mainly topologically close packed Laves phases. The BCC based HEAs are much stronger than FCC based HEAs, but many of them experience brittle to ductile transition having low ductility at room temperature, especially in the as cast condition.

As the entropy term of the Gibbs free energy decreases linearly with a decrease in temperature, high temperature SS phases are expected to become metastable at lower temperatures. Indeed, detailed microstructure analysis revealed formation of multi phase structures consisting of SS and IM phases in many HEAs after annealing and/or thermo mechanical treatment at tempera tures below 1000 1200 °C, and only few HEAs retained SS struc tures [17 21]. Unfortunately, experimental studies of equilibrium phases in HEAs at $T < 1000$ °C are challenged by slow diffusion kinetics [22]. At the same time, only alloys with no first order phase transformations in the temperature range of the application use should be selected to ensure structural stability. Therefore, equilibrium phase diagrams of these new alloys must be available.

In spite the large number, over ~200, of new MPEAs reported (i.e., in average, ~20 25 alloys per year), a vast number of com positional possibilities have yet to be explored. Indeed, the amount of alloy systems increases with factorial speed when the number of principal alloying elements increases. For example, a pallet of 27 elements results in 27 alloy systems with a single principal ele ment, 2925 alloy systems with 3 principal elements and 296,010 alloy systems with 6 principal elements. It is impossible to eval uate such huge number of alloy systems within a reasonable period of time using traditional methods. For example, if one alloy can be made and characterized in one week, it would take ~20 years to evaluate 1000 alloys, and it is not certain that some of these alloys would have properties superior to currently available commercial alloys. New approaches are required to quickly and efficiently screen promising alloy compositions for particular applications.

A strategy to design and evaluate MPEAs for structural use in the transportation and energy industries has recently been pro posed [7]. A systematic design approach uses palettes of elements chosen to meet target properties and gives methods to build MPEAs from these palettes. The developed strategy includes both single phase SS MPEAs, as well as two phase systems consisting of a SS matrix and an intermetallic phase for precipitate hardening. To systematically screen and evaluate the vast composition space offered by MPEAs and HEAs, high throughput computations and experiments with a feedback loop for validation have been sug gested [7]. The idea is to quickly reject systems with some critical property deficiency and to focus resources on characterizing the remaining systems.

In this work, we use the proposed strategy [7] to develop a methodology to quickly identify, screen and analyze hundred thousand alloy compositions for required microstructure and properties. To achieve this goal, screening criteria for alloy selection are proposed, CALPHAD calculations are used to identify the critical thermodynamic properties and microstructural fea tures, and computer programs are developed to automate alloy selection, property calculations, analysis and screening processes. Due to a huge number of possible MPEA compositions, only equiatomic MPEAs were analyzed in this work to validate the proposed screening approach. Expanding our approach to the non equiatomic composition space is our next step, which we are currently pursuing and which is beyond the scope of this paper.

2. Approaches and methods

2.1. Identification of elements and alloy properties for screening

As the first step, a master list of elements for prospective MPEA systems that can be used in intermediate temperature (MT) and high temperature (HT) applications has been identified [7]. Goal properties for these two MPEA families should exceed the char acteristic properties of Ti and Ni alloys, respectively, by a margin sufficient to warrant the extra risk and cost of development, scale up, certification and insertion. Thus the alloying elements are se lected to satisfy the requirements of the target application window based on their intrinsic properties. Starting with the periodic table of elements and excluding all non metals, halogens, noble gases, toxic and radioactive elements, semi metals (except Si), elements with the melting temperature, T_m, less than 900 °C (except low density Mg and Al), as well as extremely rare, costly, dense or compliant elements, 27 elements have been selected. These are Ag, Al, Co, Cr, Cu, Dy, Fe, Gd, Hf, Lu, Mg, Mn, Mo, Nb, Ni, Re, Rh, Ru, Sc, Si, Ta, Ti, Tm, V, W, Y, and Zr. The reasons why low density Mg and Al are left in the list are discussed in our previous paper [7]. To develop the methodology for alloy selection and to validate the approach, only equiatomic composition alloys (hereafter we call them *equiatomic alloys*) with 3 6 elements from the selected list have been evaluated in this work. Thus the processed MPEA sys tems include not only HEAs with 5 or more elements, but also 3 and 4 component MPEAs. The number of 3 , 4 , 5 , and 6 com ponent equiatomic alloys that can be produced from the selected 27 elements are 2925, 17,550, 80,730, and 296,010, respectively, i.e. 397,215 alloys.

As the second step, the alloy properties used for alloy selection and the methods to calculate these properties have been identi fied. The first set of screened properties includes thermodynamic properties of an alloy. For example, only alloys with no first order phase transformations in the temperature range of the application use should be selected to ensure structural stability. Therefore, all phase reaction temperatures, if present, must be above the max imum use temperature, T_{use}. Good ductility and fracture toughness require a solid solution (SS) primary phase, while potent strengthening mechanisms (e.g. SS and precipitation strengthen ing) may require a second (SS or intermetallic, IM) phase that can be dissolved and re precipitated above T_{use} but below solidus, T_m. The number and volume fraction of IM phases should be restricted to retain acceptable ductility and fracture toughness. Thus the temperatures and types of all solid state reactions, as well as the number and type of phases at T_m and below T_{use} should be esti mated for every selected alloy. These properties cannot be esti mated using the rule of mixtures of pure elements and CALPHAD calculations are used as outlined in the next section. For a given alloy, T_{use} is the lower of 80% of absolute T_m and the lowest tem perature below which no solid state phase reactions occur.

The second set of properties used for the alloy screening in cludes alloy density, ρ, elastic modulus, E, and cost, P. They are calculated using the rule of mixtures and the respective properties of pure elements:

$$\rho = \frac{\sum c_i M_i}{\sum c_i V_i},\ E = \frac{\sum c_i V_i E_i}{\sum c_i V_i},\ P = \frac{\sum c_i M_i P_i}{\sum c_i M_i}, \quad (1)$$

Here, c_i, M_i, V_i, E_i and P_i are the atomic fraction, molar mass, molar volume, Young's modulus and cost of element i. While the rule of mixtures works well for solid solution based alloys, errors in the calculated density and elastic modulus can be high for intermetallic phases. Reasonable screening/selection criteria can be established for these properties, depending on potential application. In the present study, the selected design properties are $\rho < 10$ g/cm^3; $E > 100$ GPa; $P <$ \$500/kg.

The third set of properties, which were calculated for all the selected alloys, are mixing enthalpy, ΔH_{mix}, of the alloying elements, and extended Hume Rothery (H R) parameters, such as atomic radius difference, δr, electronegativity difference, $\delta\chi$, and valence electron concentration difference, δ(VEC). It is thought that there are correlations between these parameters and the probability of formation of solid solution or intermetallic phases [23 28]. Rather than use this set of calculations as criteria, this work intends to determine the utility of these calculations in determining solid solutionability through comparison with CALPHAD calculations.

The following equations were used to define these parameters for the complex chemistries studied here:

$$\delta r = \sqrt{\sum c_i \left(1 - r_i / \sum c_i r_i\right)^2} \quad (2)$$

$$\delta\chi = \sqrt{\sum c_i \left(1 - \chi_i / \sum c_i \chi_i\right)^2} \quad (3)$$

$$\delta(VEC) = \sqrt{\sum c_i \left(1 - (VEC)_i / VEC\right)^2} \quad (4)$$

$$VEC = \sum c_i (VEC)_i \quad (5)$$

$$\Delta H_{mix} = \sum_{i=1}^{N} c_i \Delta H_i \equiv \sum_{i,j=1}^{N} 2 c_i c_j \omega_{ij} \quad (6)$$

Here r_i, χ_i and $(VEC)_i$ are the atomic radius, electronegativity and valence electron concentration of element i; $\Delta H_i = \sum 2 c_j \omega_{ij}$ is the concentration averaged heat of mixture of the element i with other elements in the alloy, and ω_{ij} is a concentration dependent interaction parameter between elements i and j in a sub regular solid solution model [29].

2.2. CALPHAD calculations

Integration of the CALPHAD approach with key experiments has recently been used as an effective method in the determination of phase diagrams of multicomponent alloys [30 32]. It is necessary to point out that the most of the currently available thermodynamic databases have been developed for the alloy systems based on one principal element, e.g. for Al alloys, Ni alloys, Ti alloys, etc. Use of these databases for multi principal element alloys requires extrapolation of the underlying binary data. Predictions based on this approach are approximate and subject to refinement as the databases include more ternary data. In the present work, CALPHAD calculations for an N component alloy are considered to have the highest credibility if thermodynamic data is available for all the binary and ternary systems that represent this alloy. Model parameters for subsystems higher than ternary are not considered because interactions in higher order subsystems become negligibly weak [33,34]. A reliable account of higher order systems is obtained via the extrapolation method [35].

To calculate equilibrium phase diagrams and thermodynamic properties of equiatomic alloys, Pandat v.8.1 software and Pandat thermodynamic databases, version 2013, developed by CompuTherm LLC were used. The databases and selected elements present in the databases are listed in Table 1. Based on the elements available in the databases (except PanSol), all possible 3 , 4 , 5 and 6 component equiatomic alloys were identified and 1 line phase diagram calculations (i.e. temperature as a variable) were conducted for these alloys. Due to enormous amount of 5 component and 6 component equiatomic compositions, which can be produced from the elements available in the PanSol database, the alloys for this database were created only from the elements that fall into MT and HT categories [7] (see Table 1). The maximum and minimum temperatures were selected for the calculations to be 3600 °C and 600 °C, and characteristic temperatures of the start and completion of all phase transformations occurring in this range were registered.

CALPHAD calculations were conducted for 111,654 unique equiatomic alloys, among which the amounts of 3, 4, 5 and 6 component alloys were 2521, 9803, 29,832, and 69,498, respectively (Table 2). From one to eight databases were used to calculate thermodynamic properties of a single alloy, however, the amount of the alloys calculated with multiple databases decreased rapidly with an increase in the number of databases (see Table 2), due to limited element availability in the databases (see Table 1). For example, 93,555 alloys were analyzed using 1 database, 13,101 alloys using 2 databases, 45 alloys using 7 databases, and only 1 alloy using all 8 databases. This resulted in 137,007 distinct calculations.

2.2.1. Credibility of CALPHAD calculations for studied alloys

Each of the databases, except PanSol, was developed for a particular alloy family and contains a limited number of elements typical to this alloy family. Full thermodynamic assessment of these databases is usually given only for compositions enriched with the main element. Extrapolation of the CALPHAD calculations to the equiatomic composition may be possible if all the binary and ternary systems representing this equiatomic alloy have complete thermodynamic description. The number of binary and

Table 1
Thermodynamic databases with elements included in the calculation of equilibrium phase diagrams of equi-molar composition alloys. The version of the databases is 2013.

Databases	Elements included in the analysis																								
PanAl	Ag	Al		Cr	Cu		Fe	Gd	Hf		Mg	Mn			Ni				Sc	Si		Ti		V		Y	Zr
PanCo		Al	Co	Cr			Fe						Mo		Ni	Re					Ta				W		
PanFe		Al	Co	Cr	Cu		Fe				Mg	Mn	Mo	Nb	Ni					Si		Ti		V	W		Zr
PanMo		Al		Cr			Fe		Hf			Mn	Mo			Re				Si		Ti					Zr
PanNb		Al		Cr			Fe		Hf				Mo	Nb		Re				Si		Ti			W		Zr
PanNi		Al	Co	Cr	Cu		Fe		Hf			Mn	Mo	Nb	Ni	Re		Ru		Si	Ta	Ti			W		Zr
PanTi		Al		Cr	Cu		Fe						Mo	Nb	Ni					Si	Ta	Ti		V			Zr
PanSol (MT)	Ag	Al	Co	Cr	Cu	Dy	Fe	Gd		Lu	Mg	Mn	Mo	Nb	Ni				Sc	Si		Ti	Tm	V		Y	Zr
PanSol (HT)	Ag	Al	Co	Cr					Hf				Mo	Nb	Ni	Re	Rh	Ru		Si	Ta	Ti		V	W		Zr

Table 2
Number of 3, 4, 5 and 6-component unique equiatomic alloys, which phase diagrams were calculated using different number of thermodynamic databases. The total numbers of the calculations are also shown.

Number of components	3	4	5	6
Total number of unique alloys	2521	9803	29,832	69,498
Number of unique alloys processed with *M* databases				
M 1	1353	6588	24,183	61,431
M 2	599	2039	4062	6401
M 3	272	711	1080	1302
M 4	161	308	384	307
M 5	98	121	102	49
M 6	15	20	15	7
M 7	22	16	6	1
M 8	1	0	0	0
Total number of calculations	4753	14,868	37,725	79,661

Table 3
Total number of binary and ternary systems, which represent 3-, 4-, 5-, and 6-component alloys.

Number of components	3	4	5	6
Number of binary systems	3	6	10	15
Number of ternary systems	1	4	10	20

ternary systems included in 3 , 4 , 5 , and 6 component alloys are given in Table 3. Fully credible calculations of thermodynamic equilibria, for example, for a quaternary equiatomic alloy ABCD may require assessment of all 6 binary systems (A B, A C, A D, B C, B D, C D) and 4 ternary systems (A B C, A B D, A C D, B C D). Unfortunately, not all the binaries and/or ternaries may be available in the thermodynamic databases. For example, for AlCoCrFeNi, the PanCo database contains all 10 binaries but only 2 ternaries, while the PanFe database contains 6 binaries and 3 ternaries for this same alloy. Thus, the credibility of calculated phase equilibria for AlCoCrFeNi may be different when using the PanCo and PanFe databases.

The list of binary and ternary systems assessed in thermodynamic databases can be found at the CompuTherm web site (www.computherm.com). Co and Nb are the most developed databases, but they contain limited number of elements (9 and 11, respectively). The solution database (PanSol) includes all the selected elements and contains comprehensive thermodynamic data for almost all binary systems within the selected elements. However, this database does not have thermodynamic data for ternary systems. The number of binary and ternary systems having complete thermodynamic assessments in the thermodynamic databases used in this work are given in Table 4.

To estimate credibility of the CALPHAD calculations for an alloy, we introduce two parameters: fraction of assessed binary systems ($FAB=\sum_i \kappa_i^B/TB$) and fraction of assessed ternary systems ($FAT=\sum_j \kappa_j^T/TT$). Here κ_i^B and κ_j^T are the quantities showing the levels of assessment of an *i*th binary and *j*th ternary systems, respectively, in a given database for a given alloy, while TB and TT are the total numbers of binary and ternary systems, respectively (Table 3), for a given alloy. The following values are assigned to the κ_i^B (or κ_j^T) quantities: =1 if a respective binary (or ternary) system has complete thermodynamic description in a given database; =0.1 if a respective system has a partial description; and=0 if no thermodynamic description is available.

Table 4
Number of elements and the number of binary and ternary systems assessed in given thermodynamic databases.

Database	Number of elements	Number of assessed binaries	Number of assessed ternaries
PanAl	21	21	15
PanCo	9	36	17
PanFe	21	15	10
PanMo	12	30	8
PanNb	11	46	12
PanNi	22	45	30
PanTi	18	65	1
PanSol	76	735	0

2.3. Data processing

Several application programs were developed to drive the related software packages and to analyze the resulting data. These programs (a) generate alloy compositions and batch files for CALPHAD analysis, (b) continuously run multiple batch files through the Pandat software and export critical thermodynamic data into separate text files, (c) calculate other alloy properties (such as Hume Rothery and rule of mixtures calculations), (d) create summary files containing all the screened alloys and their respective calculated properties, and (e) analyze the calculated properties against the selected criteria and identify trends pervasive to the analysis. Specifically, an AutoIt script (www.autoitscript.com) was developed for "(b)" and all other steps were performed using Visual Basic® subroutines (Visual Basic is a trademark of Microsoft Corporation). Scripts developed for "(a)" and "(d)" are given in a Supplementary information file.

3. Results

3.1. Statistical analysis of CALPHAD calculations

3.1.1. Credibility of calculations

The FAB and FAT values for the explored equiatomic alloys are given in Fig. 1. While some of the alloys have a full binary assessment (FAB=1), only 58 ternary alloy systems have a full thermodynamic assessment (FAT =1) and none of the higher order alloys have full ternary assessment (i.e. FAT < 1 for these alloys). Lacking the full set of the binaries and ternaries may lead to different levels of uncertainties of the CALPHAD results. Down selection of alloys starts by excluding all alloys with FAB=0 (no binary assessments) and alloys with the calculated solidus temperature, T_m, equal or below 600 °C.

The number of unique 3 6 component alloys with $T_m > 600$ °C and FAB > 0 are 2053, 7990, 23,212 and 50,994 (Table 5). The majority of these alloys (72,408) were calculated with a single database. Thermodynamic properties of other alloys (11,841) were

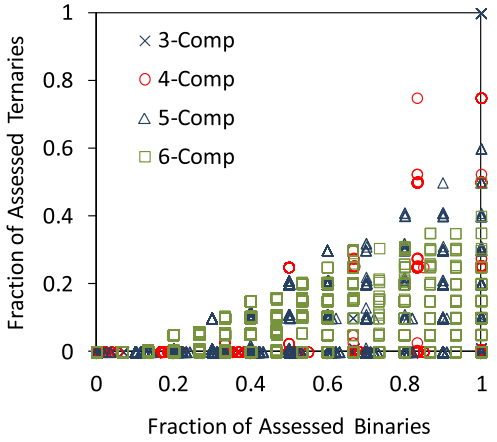

Fig. 1. Fraction of assessed binary and ternary systems for the studied 3-, 4-, 5- and 6-component alloys.

Table 5
Number of 3, 4, 5 and 6-component equiatomic alloys with $T_m > 600$ °C and FAB > 0, which phase diagrams were calculated using different number of thermodynamic (TD) databases.

Number of TD databases	Number of alloying elements			
	3	4	5	6
1	1409	5991	19,412	45,596
2	337	1277	2682	4323
3	168	473	836	886
4	83	184	221	158
5	37	37	41	24
6	17	22	16	6
7	2	6	4	1

calculated using 2 7 databases (Table 5), which allowed comparison and, in some cases for which experimental results are available, validation of the CALPHAD calculations based on the different databases. For example, all 5 elements of the AlCrFeTiZr alloy are available in 7 databases: PanAl, PanFe, PanMo, PanNb, PanNi, PanSol and PanTi. The credibility criteria as well as calculated phase diagrams for this alloy are database dependent. However, four databases that have FAB=0.7 or higher equally predict the presence of Laves and BCC phases in this alloy at T_m (see Table 6). Another example is a 4 component AlCrFeMo alloy, for which all 7 databases listed in Table 6 predict a single phase BCC structure at T_m. Four databases, PanFe, PanMo, PanNi and PanSol, with FAB ≥ 0.5, also predict the same 3 phases, 2 BCC and $AlMo_3$, at 600 °C. The third example is a 5 component AlCoCrFeNi alloy, for which thermodynamic calculations were conducted using four databases, with the PanCo and PanNi databases providing the most credible calculations (Table 6). These calculations predict three phases, B2, BCC and FCC at T_m, and B2, Sigma and BCC at 600 °C for AlCoCrFeNi. These same phases were found in experimental studies of this, AlCoCrFeNi, alloy [36 40]. We also compared the results of CALPHAD calculations with experimentally available data 65 equiatomic alloys and found good agreement for the alloys with FAB > 0.5 (see Supplementary information file). This analysis supports the validity of CALPHAD calculations with high credibility.

The distributions of the processed alloys by FAB and FAT values are given in Fig. 2. The equiatomic alloys can be arranged in 6 categories, with FAB (i) from > 0 to < 0.2, (ii) from 0.2 to < 0.4, (iii) from 0.4 to < 0.6, (iv) from 0.6 to < 0.8, (v) from 0.8 to < 1, and (vi) equal to 1. The 3 component alloys have FAB around 0.33, 0.67 and 1, with almost equal numbers of alloys in each category. The 4 to 6 component alloys are distributed almost equally in the FAB range from 0.2 to 0.8 (Fig. 2a). The fraction of alloys with FAB=1 rapidly decreases with an increase in the number of components, which is expected, as it is more difficult to achieve full thermodynamic assessment for alloys with an increasing number of components.

The most frequently observed FAT values for the processed equiatomic alloys are in the range of 0 to 0.2, and the number of alloys rapidly decreases with an increase in FAT beyond 0.2 (Fig. 2b, note the logarithmic scale for the alloy fraction). In each FAT bin, except 0.1, the fraction of alloys decreases with an increase in the number of components from 4 to 6 (Fig. 2b). The 3 component alloys fall in two FAT bins only, 0.1 and 1, as they need full thermodynamic description of only one ternary system.

3.1.2. *Distributions of equiatomic alloys by the types of phases and their compositions*

As shown in Table 7 and Fig. 3, CALPHAD calculations predict that the majority of the equiatomic alloys contain both solid solution (SS) and intermetallic (IM) phases at T_m and 600 °C. (These alloys are called SS+IM alloys in Fig. 3.) In general, there is a larger population of alloys consisting only of SS phases (SS alloys) as compared to alloys containing only IM phases (IM alloys) at T_m and 600 °C. The fractions of the SS alloys and IM alloys decrease while the fraction of SS+IM alloys increases with an increase in the number of alloying elements (Fig. 3). With a decrease in the temperature from T_m to 600 °C, the fraction of SS alloys decreases by ~30 55% (more in higher component alloys), while the fraction of IM alloys and SS+IM alloys increase (Table 7 and Fig. 3).

Fig. 4a shows nine phases that are most common in equiatomic alloys at T_m and 600 °C. These are three SS phases (BCC, HCP and FCC), three silicide phases (M_5Si_3, M_5Si_4 and M_3Si_3), an ordered B2 phase, and two Laves phases (C14 and C15). In total, 453 different phases were identified. A disordered BCC phase is the most common, and it accounts 22% and 19% of all the phases present at T_m and 600 °C, respectively. The BCC phase is also the most common

Table 6
Calculations of equilibrium phases present at T_m and 600 °C in AlCrFeTiZr, AlCrFeMo and AlCoCrFeNi equiatomic alloys using databases with different credibility values.

Alloy	Database	FAB	FAT	T_m (°C)	T_{use} (°C)	Phases at T_m	Phases at 600 °C
AlCrFeTiZr	PanAl	0.1	0	1707	901	BCC	BCC+AlZr+Al_3Zr_4
	PanFe	0.1	0	1186	671	2 Laves+BCC	2 Laves+B2+$AlTi_3$
	PanMo	0.7	0.1	1342	682	Laves+BCC	Laves+AlZr+Al_3Zr_4+BCC
	PanNb	0.7	0	1154	634	Laves+BCC	2 Laves+$TiAl_2$+HCP
	PanNi	0.2	0	1137	602	2 Laves+BCC	2 Laves+BCC+$AlTi_3$
	PanSol	1.0	0	1005	665	BCC+Laves+AlZr	BCC+2 Laves+AlZr
	PanTi	0.7	0	1201	750	BCC+Laves	2 Laves+Al_2Zr_3+$AlTi_3$
AlCrFeMo	PanCo	1.0	0.0	1482	1131	BCC	BCC +A15+L12
	PanFe	0.5	0.3	1528	604	BCC	2 BCC +$AlMo_3$
	PanMo	1.0	0.0	1461	612	BCC	2 BCC+$AlMo_3$
	PanNb	0.3	0.0	1474	829	BCC	BCC+Al_8Cr_5
	PanNi	0.7	0.0	1469	818	BCC	2 BCC +$L1_2$
	PanSol	1.0	0.0	1525	637	BCC	2 BCC+$AlMo_3$
	PanTi	0.7	0.0	1469	1047	BCC	BCC +$AlMo_3$
AlCoCrFeNi	PanCo	1.0	0.2	1265	632	B2+BCC+FCC	B2+Sigma+BCC
	PanFe	0.6	0.2	1175	656	B2+FCC	B2+Sigma+BCC
	PanNi	0.9	0.4	1237	623	B2+BCC+FCC	B2+Sigma+BCC
	PanSol	1.0	0	1170	629	B2+FCC	B2+BCC+BCC

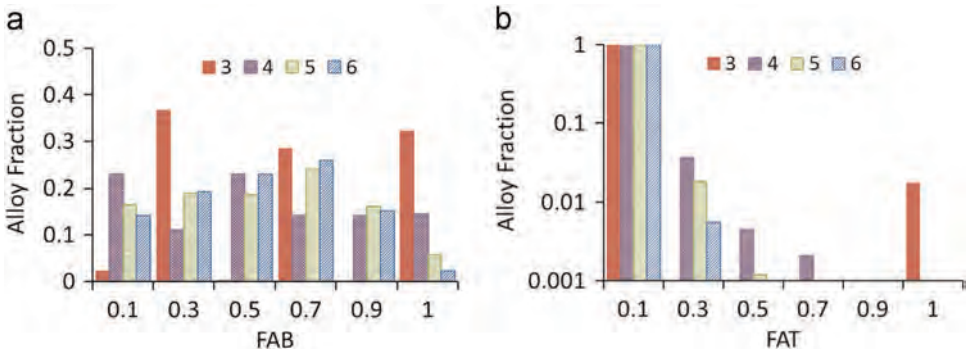

Fig. 2. Distribution of the processed equiatomic N-component alloys (with $T_m > 600$ °C and FAB > 0) by the fraction of assessed binary (FAB) and ternary (FAT) systems.

Table 7
The number of 3, 4, 5, and 6-component equiatomic alloys with different phase contents at T_m and 600 °C.

Number of components	3	4	5	6
Total number of analyzed alloys	2053	7990	23,212	50,994
Alloys with only SS phases at T_m	954	2442	4275	5458
Alloys with only IM phases at T_m	284	934	1803	2766
Alloys with SS+IM phases at T_m	815	4614	17,134	42,770
Alloys with only SS phases at 600 °C	616	1300	2043	2284
Alloys with only IM phases at 600 °C	259	945	2005	3200
Alloys with SS+IM phases at 600 °C	1178	5745	19,164	45,510

in the SS equiatomic alloys (Fig. 4b). It accounts for 62% of all phases at T_m and 48% at 600 °C. The second is an HCP phase (26% and 36%) and the third is an FCC phase (12% and 15%). The remaining 0.1% at 600 °C is a cubic diamond phase (not shown in the figure).

Fig. 5 shows how different categories of 3 6 component equiatomic alloys are distributed by the number of phases at the solidus (T_m) temperature. Almost all single phase alloys are SS alloys. The amount of single phase IM alloys is very small (< 1%) and they all are 3 component alloys. The fraction of single phase alloys considerably decreases with an increase in the number of alloying elements. For example, in 3, 4, 5 and 6 component alloys the fractions of the single phase SS alloys are 26%, 13.4%, 6.9% and 3.7%, respectively. Almost all SS alloys contain from 1 to 3 phases and almost all N component IM alloys contain from (N 2) to N phases. The SS+IM alloys may contain from 2 to N phases.

The frequency with which a given alloying element appears in all analyzed alloys is generally different from the frequency of occurrence in SS alloys (Fig. 6). This indicates that some elements are more commonly associated with SS phases. The elements that more often appear in SS phases at T_m are Al, Cr, Hf, Mg, Mn, Mo, Nb, Re, Rh, Ru, Ta, Ti, V and W. The elements that appear less frequently in SS alloys are Fe, Ni, Sc, Si, Y and Zr. Moreover Si is completely absent in SS alloys. The third group of elements is neutral to SS phase formation and is equally distributed in SS and all other alloys. These are Ag, Co, Cu, Dy, Gd, Hf, Lu, and Tm.

3.1.3. Solidus and maximum use temperatures

Solidus, T_m, and maximum use temperatures, T_{use}, are important quantities for structural materials. In conventional alloys, the solidus temperature is generally directly related to a critical temperature, $T_c \approx 0.6$ $0.8T_m$, above which alloy structural properties rapidly degrade, while the maximum use temperature is the temperature below which the alloy does not experience 1st order phase transformations. Thus increasing both T_m and T_{use} is beneficial as an alloy can be used in a wider temperature range and at higher temperatures.

Cumulative distributions of the analyzed equiatomic alloys by their T_m and T_{use} are shown in Figs. 7a and b, respectively. In both cases, the fraction of the alloys decreases rapidly with an increase in T_m or T_{use}, and the rate of the decrease is higher for the higher component alloys. For example, the fractions of 3 and 6 component alloys with $T_m > 1200$ °C are 58% and 25%, respectively, while the fractions of these alloy types with $T_m > 1800$ °C are only 13% and 1.6% (Fig. 7a). The fractions of 3 , 4 , 5 and 6 component alloys with $T_{use} > 1200$ °C decrease geometrically, by more than a factor of 2, for each increase in the number of elements (16%, 6.6, 3.3% and 1.6% respectively). As shown in Fig. 7b the number of alloys with $T_{use} > 1800$ °C decreases geometrically, by approximately an order of magnitude, for each increasing element (0.8%, 0.2%, 0.05% and 0.005%, respectively).

In each category of equiatomic alloys, SS alloys show the maximum T_m and T_{use} values. Specifically, for the 3, 4, 5 and 6 component equiatomic alloys the maximum T_m values of 2925 °C, 2829 °C, 2692 °C, and 2481 °C and maximum T_{use} values of 2285 °C, 2209 °C, 2099 °C and 1931 °C are observed in the BCC SS alloys MoTaW, MoNbTaW, MoNbReTaW and MnMoNbReTaW,

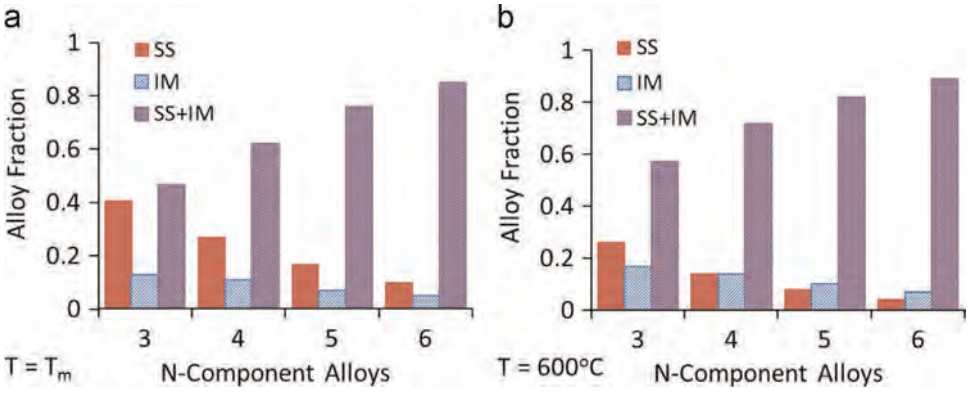

Fig. 3. Fraction of N-component SS, IM and SS+IM alloys at (a) T T_m and (b) T 600 °C.

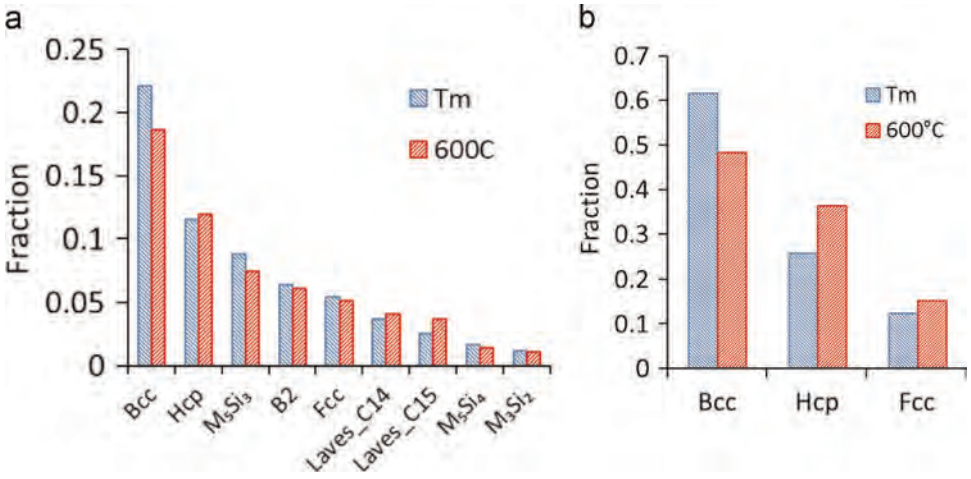

Fig. 4. The most commonly observed phases in (a) all processed equiatomic alloys and (b) SS alloys at T T_m and 600 °C.

respectively.

3.2. Density, Young's modulus and cost of the processed equiatomic alloys

The cumulative distributions of the fractions of equiatomic al loys by their density, Young's modulus and cost are given in Fig. 8. The alloy density varies from 2.37 to 18 g/cm^3. The minimum density increases and the maximum density decreases with an increase in the number of alloying elements. For example, the lowest density among the three component alloys is 2.37 g/cm^3 (MgScSi), while among the 6 component alloys, it is 3.19 g/cm^3 (AlMgScSiTiV). At the same time, the maximum density for the 3 component alloys is 18.9 g/cm^3 (ReTaW) and for the 6 compo nent alloys is 15.8 g/cm^3 (HfReRhRuTaW). About 75% of all the analyzed alloys have the density below 10 g/cm^3 and from 10% to 24% of the alloys (the alloy fraction decreases with an increase in the number of alloying elements) have the density below 6 g/cm^3 (Fig. 8a).

The Young's modulus ranges from 54 GPa (MgSiY, MgSiZr and GdMgSiY) to 439 GPa (ReRuW). The upper limit decreases no ticeably with an increase in the number of alloying elements. For example, the maximum Young's modulus values among the 4 , 5 and 6 component alloys are 411 GPa (MoReRuW), 389 GPa

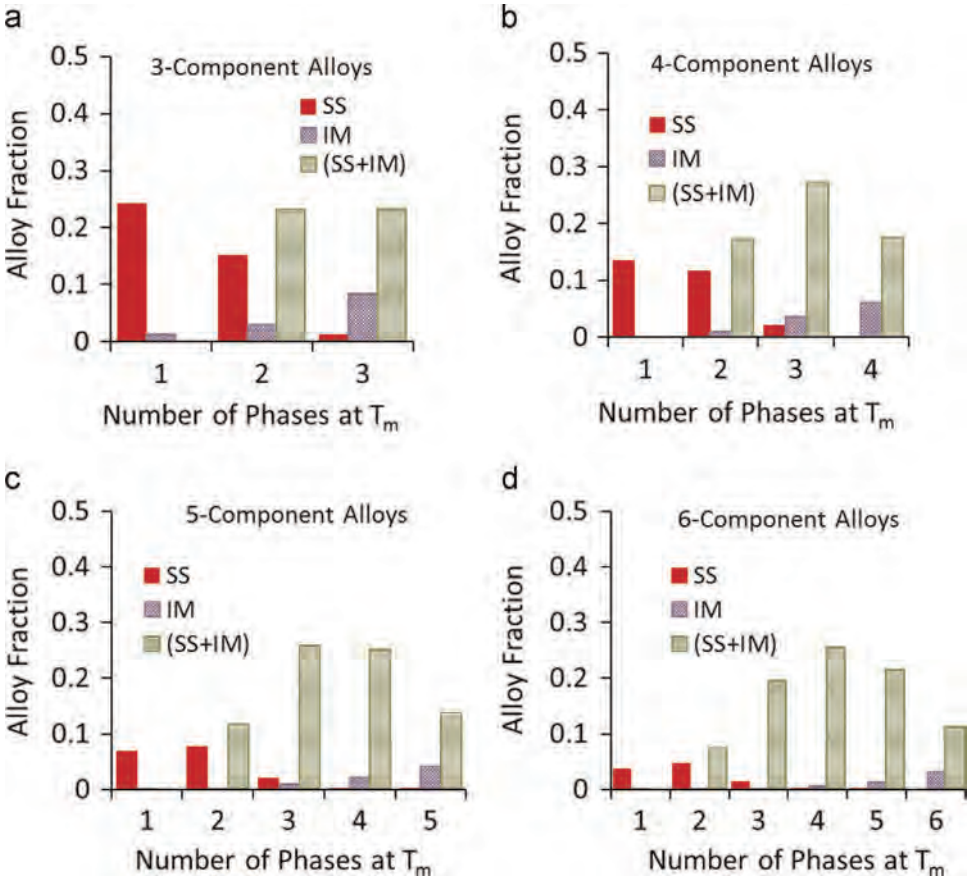

Fig. 5. Distributions of the N-component equiatomic alloys by the number of phases at T_m.

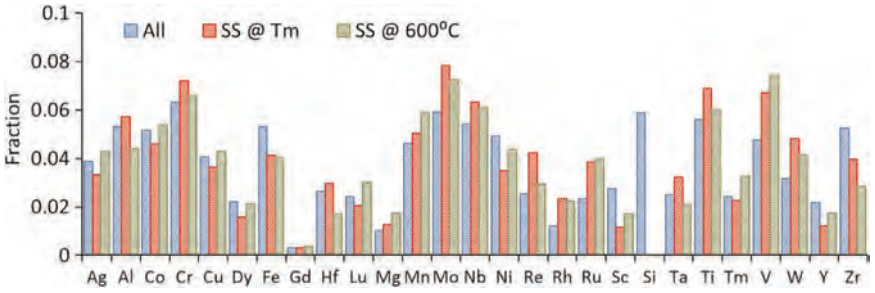

Fig. 6. Distributions of the alloying elements in all processed equiatomic alloys and in alloys with only SS phases at T_m or 600 °C.

(CrMoReRuW), and 370 GPa (CrMoReRhRuW), respectively. More than 70% of the processed alloys have moduli above 100 GPa and about 15% of the alloys have moduli above 200 GPa (Fig. 8b).

The alloy cost spread varies by over 4 orders of magnitude, from $3/kg to over $100,000/kg. The cost of ~39% of all the processed alloys is less than $1000/kg, ~30% is less than $500/kg and ~14% is less than $100/kg. The cost of the alloys generally increases with an increase in the number of alloying elements. For example, ~40% of the 3 component alloys and only 26% of the 6 component alloys cost $500/kg or less.

3.3. Alloy selection process

Having the library of equiatomic alloys and their calculated thermodynamic and physical properties, we can identify alloys that satisfy a specific set of requirements. These selection criteria can be established to identify potential compositions that would meet application requirements or could be used for further alloy development. To illustrate this process of alloy selection, we apply five criteria, one after another, to identify multi component equiatomic alloys with (i) a single phase SS phase at T_m, (ii) maximum use temperature above 1000 °C, (iii) Young's modulus above 100 GPa, (iv) cost less than $500 per kg and (v) density less than 10 g/cm^3. Compositions and properties of some of these alloys are given.

3.3.1. Equiatomic alloys with a single SS phase at T_m

Among 13,129 SS equiatomic alloys identified at T_m, 5,293 (i.e. ~40%) are single phase solid solutions, from which 548 are 3 component, 1149 are 4 component, 1647 are 5 component and 1949 are 6 component alloys. The distributions of the single phase SS alloys by the number of components and types of phases at T_m are given in Table 8. The majority of the single phase SS alloys have BCC structures (4538 alloys). The amounts of HCP and FCC alloys are considerably lower, 621 and 134, respectively. The fraction of BCC alloys increases (from 73% to 92%) and the fractions of the HCP and FCC alloys decrease (from 18% to 7% and 9% to 1%, respectively) with an increase in the number of components from 3 to 6. Among the single phase FCC alloys, 48 are 3 component, 41 are 4 component, 32 are 5 component and 13 are 6 component alloys.

Compositions and some properties of 5 and 6 component equiatomic alloys that are single phase FCC structures at T_m, are given in Tables 9 and 10, respectively. The density, modulus and cost of these alloys are in the range from 7.6 g/cm^3 to 12.0 g/cm^3, 125 GPa to 317 GPa, and $10/kg to $30,403/kg, respectively. Many of these FCC alloys experience phase transformations at temperatures below T_m, which result in reduced maximum use temperature, $T_{use} < 900$ °C, and several phases below T_{use}. Only one 6 component FCC alloy (CoCuFeMnNiRe) and three 5 component FCC alloys (CoCrMoNiRh, CoFeMnNiRu, and CoFeMnReRu) have $T_{use} > 1000$ °C. These 4 alloys have two phase, FCC+HCP, structures below T_{use}. Phases in the CoCrFeMnNi alloy were calculated using three databases, Fe, Ni and Solution, and in CoFeMnMoNi and CoFeMnNiV using two databases, Ni and Solution, and Fe and Solution, respectively, with FAB values ranging from 0.3 to 1.0. Comparison of the results of these calculations shows satisfactory agreement between the thermodynamic databases (see Table 9). Among the alloys listed in Tables 9 and 10, only three alloys were reported in open literature. These are CoCrCuFeNi [41,42], CoCrFeMnNi [4,6,43] and CoCrCuFeMnNi [6]. Phases predicted in these alloys are in good agreement with the phases reported from experimental studies (see Supplementary information file).

3.3.2. Equiatomic alloys with a single SS phase at T_m, $T_{use} > 1000$ °C and $E > 100$ GPa

Applying an additional criterion, $T_{use} > 1000$ °C, reduces the number of single phase SS alloys to 1455, with a stronger decrease in the number of alloys having larger number of alloying elements (Table 8). About 81% of these alloys are BCC, 17% are HCP and only 2% are FCC structures. Additionally applying the modulus restriction ($E > 100$ GPa) reduces the number of the selected alloys to 1282, due to a decrease in the number of alloys with BCC and HCP structures, while the number of FCC alloys does not change

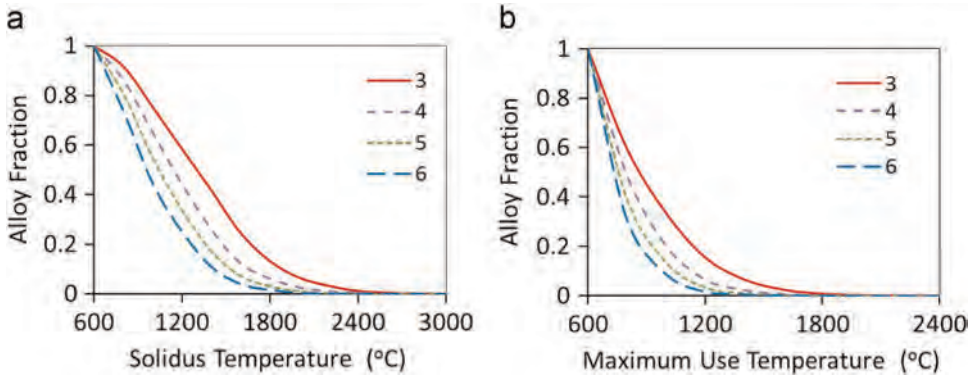

Fig. 7. Cumulative distributions of 3–6 component equiatomic alloys by (a) solidus temperature and (b) maximum use temperature.

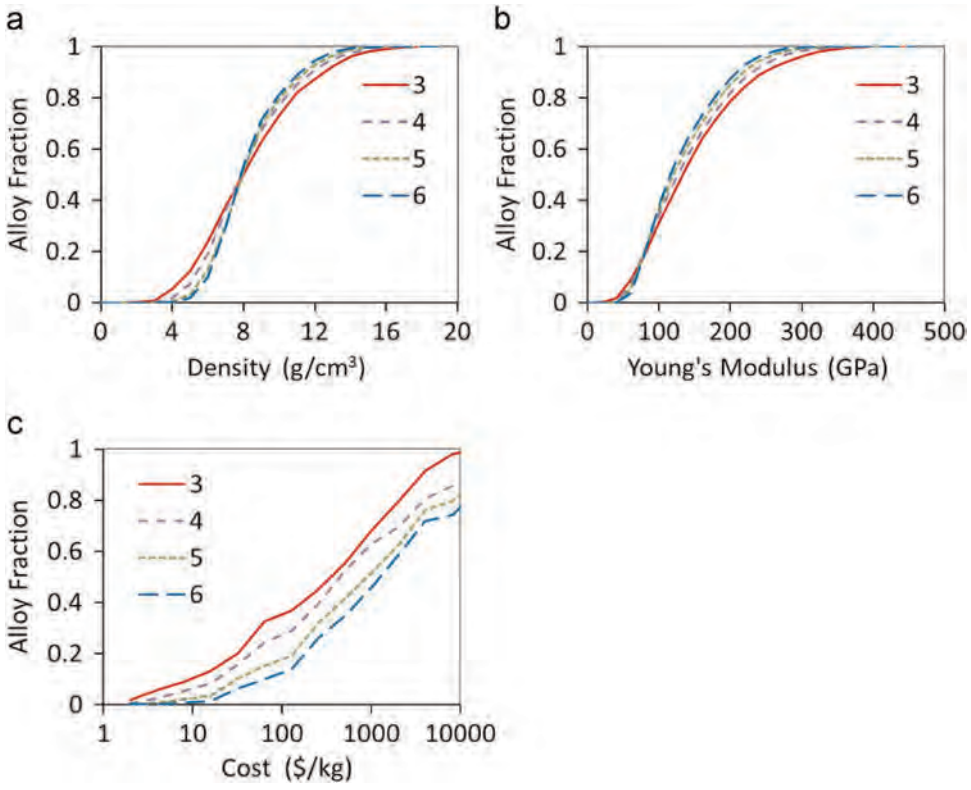

Fig. 8. Cumulative distributions of the processed 3–6 component equiatomic alloys by (a) alloy density, (b) Young's modulus and (c) cost.

Table 8
The number of 3, 4, 5, and 6-component equiatomic alloys, which are single-phase BCC, HCP or FCC solid solutions at T_m and have $T_{use} > 1000$ °C, $E > 100$ GPa and $P <$ \$500/kg.

Phase ID\Number of components	3	4	5	6
Single-phase solid solutions	548	1149	1647	1949
BCC	404	909	1426	1799
HCP	96	199	189	137
FCC	48	41	32	13
$+T_{use} > 1000$ °C	229	349	433	444
BCC	162	278	352	388
HCP	52	61	78	55
FCC	15	9	3	1
$+E > 100$ GPa	193	316	377	396
BCC	134	266	343	383
HCP	44	41	31	12
FCC	15	9	3	1
$+P <$ \$500/kg	77	107	117	110
BCC	74	105	117	110
HCP	0	0	0	0
FCC	3	2	0	0
$+\rho < 10$ g/cm^3	50	75	79	73
BCC	47	73	79	73
HCP	0	0	0	0
FCC	3	2	0	0

(Table 8). Compositions of 4 component FCC alloys and 5 and 6 component HCP alloys that satisfy these criteria are shown in Tables 11, 12 and 13, respectively. Almost all these alloys have single phase or two phase structures and only two alloys have three phases below T_{use}. As T_{use} is identified as a temperature below which no first order phase reactions occur and the alloys are single phase structures at T_m, the existence of two or three phases below T_{use} indicates that the secondary phases can be dissolved and re precipitated at temperatures between T_{use} and T_m, and thus these alloys can be heat treatable. Among the alloys shown in Tables 11, 12 and 13, only one, CoCrFeNi was studied experimen tally [37,44], and the calculated and experimental data for this alloy agree very well. All alloys having a single phase HCP struc ture at T_m, $T_{use} > 1000$ °C and $E > 100$ GPA contain rare earth ele ments, as well as Re, Rh and/or Ru, and are very expensive, with the cost exceeding \$1,600 per kg.

3.3.3. *Equiatomic alloys with a single SS phase at T_m, $T_{use} > 1000$ °C, $E > 100$ GPa, $P <$ \$500/kg and $\rho < 10$ g/cm^3*

Adding a restriction by cost ($P <$ \$500/kg) reduces the number of alloys to 411 (Table 8). Almost all these alloys are BCC structures at T_m. None of the HCP alloys and only 6 FCC alloys, among which 3 (CoMoNi, CoCrNi and CoCuNi) are 3 component and 2 (CoCrFeNi and CoFeMoNi, Table 11) are 4 component alloys, meet these cri teria. CoCrNi and CoCuNi retain the single phase FCC structure down to room temperature, while CoMoNi has two phase struc ture (FCC+μ) below 1000 °C. The single phase FCC structure of CoCuNi was reported earlier [45], in good agreement with the CALPHAD calculations.

The cumulative distribution of the 411 selected single phase SS alloys by the alloy density is given in Fig. 9. The alloy density is in the range from 4.0 g/cm^3 to 16 g/cm^3. About 70% of the down selected alloys have densities below 10 g/cm^3, 44% have densities below 8 g/cm^3, and ~11% have densities below 6 g/cm^3. The compositions, as well as some of their calculated properties, of the selected 5 and 6 component BCC alloys with densities less than 10 g/cm^3 and FAB > 0.7 are given in Tables 14 and 15.

Table 9
5-component equiatomic alloys which, in accord to CALPHAD calculations, are single-phase FCC structures at T_m. The database used for calculations, FAB values and some calculated properties are also shown.

Alloy	Database	*FAB*	T_m (°C)	T_{use} (°C)	Phases at 600 °C	ρ (g/cm^3)	*E* (GPa)	*Cost* ($/kg)
AgCuFeHfNi	PanAl	0.1	1236	934	Fcc+Hcp	10.4	127	4869
AgCuHfMnNi	PanAl	0.1	1116	838	Fcc+Hcp	10.4	125	4879
AgFeHfMnNi	PanAl	0.1	1297	983	Fcc+Hcp	10.2	138	4960
CoCrCuFeNi	PanNi	0.6	1308	781	Fcc+Fcc	8.3	206	12
CoCrCuMnNi	PanNi	0.3	1186	621	Fcc+Fcc	8.2	203	12
CoCrCuMoNi	PanNi	0.6	1286	780	Fcc+Bcc+ μ	8.9	236	42
CoCrFeMnNi	PanFe	0.6	1285	627	Fcc+Bcc	8.0	220	11
CoCrFeMnNi	PanNi	0.6	1290	977	Fcc	8.0	220	11
CoCrFeMnNi	PanSol	1.0	1249	726	Fcc+Bcc	8.0	220	11
CoCrFeMnSn	PanFe	0.3	750	545	Fcc+CoSn+Bcc	7.6	161	14
CoCrFeMnTm	PanSol	0.6	1264	956	Fcc+Hcp	8.2	164	30,277
CoCrFeNiTm	PanSol	0.6	1359	842	Fcc+Hcp	8.4	164	29,990
CoCrMnNiTm	PanSol	0.6	1238	875	Fcc+Hcp	8.4	162	30,059
CoCrMoNiRh	PanSol	0.7	1403	1067	Fcc+Bcc	9.7	265	9351
CoCrNiTmV	PanSol	0.6	1105	791	Fcc+Bcc+Hcp	8.1	150	30,396
CoCuFeMnNi	PanNi	0.3	1178	630	Fcc+Fcc+Bcc	8.4	189	11
CoCuFeMnRe	PanNi	0.3	1378	775	Fcc+Hcp+Fcc	11.3	253	1299
CoCuFeMnRu	PanNi	0.1	1284	973	Fcc+Hcp	9.2	245	752
CoCuFeMoNi	PanNi	0.6	1294	697	Fcc+Bcc+Fcc+ μ	9.0	223	41
CoFeMnMoNi	PanNi	0.6	1272	963	Fcc+ μ	8.7	236	41
CoFeMnMoNi	PanSol	0.9	1237	749	Fcc+Bcc+ μ	8.7	236	41
CoFeMnMoTm	PanSol	0.5	1320	646	Hcp+ μ	8.8	178	27,239
CoFeMnNiRu	PanNi	0.4	1391	1058	Fcc+Hcp	9.2	260	764
CoFeMnNiTm	PanSol	0.6	1275	966	Fcc	8.5	151	29,767
CoFeMnNiV	PanFe	0.3	1158	871	Fcc	7.8	187	50
CoFeMnNiV	PanSol	1.0	1133	852	Fcc	7.8	187	50
CoFeMnReRu	PanNi	0.3	1639	1257	Fcc+Hcp	12.0	317	1737
CoFeMnTmV	PanSol	0.6	1143	623	Fcc+Bcc	8.0	141	30,386
CoFeMoNiTm	PanSol	0.6	1340	789	Fcc+Hcp+ μ	9.0	178	27,007
CoFeNiTmV	PanSol	0.6	1208	912	Fcc	8.2	140	30,098
CoMnMoNiTm	PanSol	0.5	1243	703	Fcc+Bcc+Hcp	8.9	177	27,063
CoMnNiTmV	PanSol	0.6	1161	874	Fcc	8.2	138	30,168
CoMoNiTmV	PanSol	0.6	1226	651	Fcc+Bcc+Hcp	8.7	165	27,338
CrFeMnNiTm	PanSol	0.6	1231	853	Fcc+Hcp	8.2	163	30,293
CuFeHfMnNi	PanAl	0.3	1216	858	Fcc+Hcp+Fcc	9.9	150	5295
CuFeMnNiRu	PanNi	0.2	1246	942	Fcc+Hcp	9.2	244	750
FeMnNiTmV	PanSol	0.6	1121	842	Fcc	8.0	139	30,403

Table 10
6-component equiatomic alloys which, in accord to CALPHAD calculations, are single-phase FCC structures at T_m. The database used for calculations, FAB values and some calculated properties are also shown.

Alloy	Database	*FAB*	T_m (°C)	T_{use} (°C)	Phases at 600 (°C)	ρ (g/cm^3)	*E* (GPa)	*Cost* ($/kg)
AgCuFeHfMnNi	PanAl	0.2	1153	750	Fcc+Hcp+Fcc	10.0	137	4354
CoCrCuFeMnNi	PanNi	0.4	1205	620	Fcc+Fcc+Bcc	8.2	205	10
CoCrCuFeMoNi	PanNi	0.7	1300	684	Fcc+Bcc+σ+μ	8.7	232	36
CoCrFeMnMoNi	PanNi	0.7	1286	689	Fcc+ σ + μ	8.5	243	36
CoCrFeMnNiTm	PanSol	0.7	1265	721	Fcc+Hcp	8.3	168	26,324
CoCrFeMoNiTm	PanSol	0.7	1281	610	Hcp+Bcc+ μ	8.7	191	24,144
CoCrMnMoNiTm	PanSol	0.6	1226	926	Fcc+Bcc+Hcp	8.7	190	24,189
CoCuFeMnMoNi	PanNi	0.4	1215	679	Fcc+Bcc+Fcc+ μ	8.8	219	35
CoCuFeMnNiRe	PanNi	0.4	1329	1008	Fcc+Hcp	10.9	245	1142
CoCuFeMnNiRu	PanNi	0.3	1301	986	Fcc+Hcp	9.1	238	641
CoFeMnMoNiTm	PanSol	0.6	1268	611	Fcc+Bcc+Hcp	8.8	181	23,999
CoFeMnNiTmV	PanSol	0.7	1171	882	Fcc	8.1	148	26,410
CoFeMoNiTmV	PanSol	0.7	1199	905	Fcc+Bcc	8.6	171	24,218

3.4. Application of Hume Rothery rules to multiprincipal element alloys

The original Hume Rothery rules for extended substitutional solid solutions give four conditions: (i) the atomic radii of the solute and solvent atoms differ by no more than 15%, (ii) the crystal structures of solute and solvent are identical, (iii) the elements have the same valency and (iv) similar electronegativity [46]. In the case of MPEAs, the second condition becomes less restrictive and solid solutions can also form in alloys consisting of elements with different crystal structures [5,11]. Fig. 10 shows distributions of the calculated SS, IM and SS+IM MPEAs by the atomic radius difference, Δr (Fig. 10a), electronegativity difference, $\Delta\chi$ (Fig. 10b), and valence electron concentration difference, Δ(VEC) (Fig. 10c). SS alloys are in the Δr range from 0 to 15% and at $\Delta r > 15\%$ only IM and SS+IM alloys are present (Fig. 10a). Therefore, the first Hume Rothery condition applies. The majority of SS alloys have Δr below 8%. The majority of IM alloys have Δr above 8%, but some of them have Δr as low as 4 6% (Fig. 10a). The

Table 11
4-component equiatomic alloys which, in accord to CALPHAD calculations, are single-phase FCC structures at T_m and have $T_{use} > 1000$ °C and $E > 100$ GPa. The databases used for calculations, FAB values and some calculated properties are also shown.

Alloy	Database	*FAB*	T_m (°C)	T_{use} (°C)	Phases at 600 °C	ρ (g/cm^3)	E (GPa)	*Cost* ($/kg)
CoCrFeNi	PanNi	1.0	1422	1083	Fcc	8.2	226	13
CoCrNiRh	PanSol	0.7	1527	1167	Fcc	9.5	244	12,605
CoCrNiTm	PanSol	0.5	1355	1029	Fcc+Hcp	8.6	155	34,937
CoFeMnRu	PanNi	0.2	1471	1025	Fcc+Hcp	9.2	273	926
CoFeMoNi	PanFe	1.0	1377	1047	Fcc+μ	9.1	245	48
CoFeMoNi	PanNi	1.0	1338	1016	Fcc+μ	9.1	245	48
CoFeNiRu	PanNi	0.7	1551	1186	Fcc+Hcp	9.6	276	916
CoFeNiTm	PanSol	0.5	1404	1068	Fcc	8.7	142	34,543
CoMnNiRu	PanNi	0.3	1371	1042	Fcc+Hcp	9.5	272	920
CoNiRhV	PanSol	0.7	1407	1071	Fcc	9.1	203	12,693
FeMnNiRu	PanNi	0.3	1349	1025	Fcc+Hcp	9.3	271	924

Table 12
5-component equiatomic alloys which, in accord to CALPHAD calculations, are single-phase HCP structures at T_m, with $T_{use} > 1000$ °C and $E > 100$ GPa. The database used for calculations, FAB values and some calculated properties are also shown.

Alloy	Database	*FAB*	T_m (°C)	T_{use} (°C)	Phases at 600 °C	ρ (g/cm^3)	E (GPa)	*Cost* ($/kg)
AgLuMnMoTm	PanSol	0.1	1338	1016	Hcp+Bcc	9.4	126	118,489
CoCrCuReRu	PanNi	0.4	1637	1255	Hcp	12.1	318	1720
CoCrDyLuTm	PanSol	0.1	1466	1118	Hcp	8.8	103	115,708
CoCrFeReRu	PanNi	0.7	1547	1183	Hcp	11.9	333	1749
CoCrHfReRu	PanSol	0.5	1430	1089	Hcp+C15	13.0	275	5153
CoCrHfRhRu	PanSol	0.3	1419	1081	Hcp+C15	11.3	237	11,879
CoCrLuMnTm	PanSol	0.3	1343	1020	Hcp	8.8	129	139,900
CoCrLuMoTm	PanSol	0.3	1421	1018	Hcp+Bcc	9.2	152	129,504
CoCrLuNiTm	PanSol	0.3	1385	1053	Hcp	9.0	128	138,876
CoCrNiReRu	PanSol	0.8	1500	1039	Hcp+Fcc	12.2	333	1739
CoCrReRhRu	PanSol	0.4	1802	1387	Hcp	12.8	343	8434
CoHfMoReRu	PanSol	0.5	1843	1091	Hcp+C15	13.3	286	4804
CoHfMoRhRu	PanSol	0.3	1668	1247	Hcp+C15	11.7	249	10,926
CoHfReRhRu	PanSol	0.1	2111	1634	Hcp	13.8	275	10,203
CoLuMnNbTm	PanSol	0.1	1322	1003	Hcp+Bcc	8.9	107	129,536
CoLuMoNiTm	PanSol	0.3	1353	1028	Hcp	9.4	142	127,947
CrCuReRuZr	PanNi	0.2	1613	1236	Hcp	10.9	257	1894
CrDyLuMoTm	PanSol	0.1	1544	1151	Hcp+Bcc	9.0	123	109,178
CrFeHoLuTm	PanSol	0.1	1366	1038	Hcp	8.8	105	117,944
CrHfReRhRu	PanSol	0.3	1572	1203	Hcp+C15	13.5	285	10,315
CrHoLuNiTm	PanSol	0.1	1423	1084	Hcp	8.9	104	117,402
CrLuMnMoTm	PanSol	0.2	1469	1121	Hcp+Bcc	9.0	151	130,447
CrMoNiReRu	PanSol	0.9	1466	1022	Hcp+Bcc+Fcc	12.3	352	1627
CrMoReRhRu	PanSol	0.5	1880	1376	Hcp+Bcc	12.8	361	7870
CrNiReRhRu	PanSol	0.6	1637	1006	Hcp+Fcc	12.8	342	8436
DyLuMoTiTm	PanSol	0.1	1560	1193	Hcp+Bcc	8.6	107	109,865
FeHoLuMoTm	PanSol	0.1	1444	1101	Hcp+Bcc	9.2	117	110,114
HfMoReRhRu	PanSol	0.3	2062	1012	Hcp+C15	13.8	294	9648
HfReRhVZr	PanSol	0.1	1948	1504	Hcp	11.5	178	10,343
HoLuMoNiTm	PanSol	0.1	1463	1116	Hcp+Bcc	9.3	115	109,641
LuMoScTiTm	PanSol	0.2	1451	1106	Hcp+Bcc	7.4	112	135,076

Table 13
6-component equiatomic alloys which, in accord to CALPHAD calculations, are single-phase HCP structures at T_m, with $T_{use} > 1000$ °C and $E > 100$ GPa. The database used for calculations, FAB values and some calculated properties are also shown.

Alloy	Database	*FAB*	T_m (°C)	T_{use} (°C)	Phases at 600 °C	ρ (g/cm^3)	E (GPa)	*Cost* ($/kg)
CoCrHfReRhRu	PanSol	0.3	1596	1032	Hcp+C15	12.9	275	9423
CoCrMoReRhRu	PanSol	0.5	1696	1104	Hcp+Bcc	12.3	340	7096
CoCrReRhRuV	PanSol	0.4	1470	1121	Hcp+Bcc	11.6	305	7676
CrDyHoLuMoTm	PanSol	0.1	1536	1174	Hcp+Bcc	9.0	111	88,930
CrDyLuMoTmY	PanSol	0.1	1490	1138	Hcp+Bcc	8.0	110	96,125
CrDyLuMoTmZr	PanSol	0.1	1356	1030	Hcp+Bcc+C15	8.6	114	96,012
CrFeHoLuMoTm	PanSol	0.2	1404	1069	Hcp+Bcc	9.0	132	102,080
CrHoLuMoNiTm	PanSol	0.2	1433	1092	Hcp+Bcc	9.1	130	101,674
DyLuMoScTiTm	PanSol	0.1	1467	1119	Hcp+Bcc	7.6	102	103,666
DyLuMoTiTmZr	PanSol	0.1	1446	1102	Hcp+Bcc	8.2	101	96,542
FeHoLuMoNiTm	PanSol	0.2	1359	1033	Hcp+Bcc	9.1	124	101,129
HoLuMoNiScTm	PanSol	0.1	1477	1127	Hcp+Bcc	8.2	108	103,572

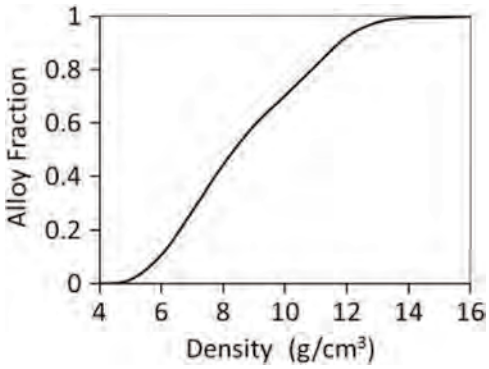

Fig. 9. Cumulative distribution of 3–6 component equiatomic alloys, which are single-phase SS at T_m, have $T_{use} > 1000$ °C, $E > 100$ GPa, and cost < \$500/kg, by the alloy density.

SS+IM alloys have a wide range of Δr, from ~3% to 20%, with high population between 8% and 14%.

SS, IM and SS+IM alloys have similar $\Delta\chi$ distributions, showing that electronegativity difference has little effect on SS phase formation in MPEAs (Fig. 10b). $\Delta\chi$ values are between 0 and 30%, with the majority of the alloys having $\Delta\chi$ between 10% and 20%. At the same time, a clear separation of SS and IM alloys by Δ(VEC) values is seen (Fig. 10c). In particular, SS alloys are present in the Δ(VEC) range from 0 to 55% with a peak at ~20 30%, while IM alloys are present in the Δ(VEC) range from 15 to 75%, with a peak at ~40 50%. The behavior of SS+IM alloys is similar to that of the IM alloys. At Δ(VEC) < 10%, only SS alloys are present and at Δ(VEC) > 60%, only IM and SS+IM alloys are present (Fig. 10c). From this analysis, formation of SS in MPEAs does not require similar electronegativity and similar valency of the alloying elements.

Recent publications use enthalpy of mixing, ΔH_{mix}, as an additional parameter, for predicting the formation of SS or IM phases in HEAs [28,47,48]. Explicit use of the CALPHAD approach allows for a self consistent balance of the thermodynamic factors controlling which phases are present at equilibrium. Nevertheless for completeness the distributions of SS, IM and SS+IM MPEAs by ΔH_{mix} values are shown in Fig. 10d. SS alloys have ΔH_{mix} in the range of 50 kJ/mol to 25 kJ/mol, with the most frequently observed values of $20 < \Delta H_{mix} < 10$ kJ/mol. The IM alloys have ΔH_{mix} in the range from 70 kJ/mol to 10 kJ/mol, with the most frequently observed values of $40 < \Delta H_{mix} <$ 10 kJ/mol. Thus, IM alloys tend to have more negative values of ΔH_{mix} than SS alloys and none of the IM alloys have $\Delta H_{mix} > 10$ kJ/mol. The SS+IM MPEAs are present within the ΔH_{mix} range that covers both SS and IM alloys (Fig. 10d).

The MPEAs considered here include not only HEAs (equiatomic alloys with 5 and 6 components), but also equiatomic alloys with 3 and 4 components. Therefore, it is interesting to see how different are the Δr and ΔH_{mix} values for these alloy categories. The fractions of the N component SS and IM alloys having different Δr values are given in Fig. 11a and b, respectively. With an increase in N, the peak positions of the distributions have a tendency to shift toward slightly higher Δr values, both for the SS and IM alloys. The fractions of the *N* component SS and IM alloys having different ΔH_{mix} values are given in Fig. 11c and d, respectively. The alloys with different number of alloying elements have almost the same distributions by ΔH_{mix}.

Table 14
5-component equiatomic alloys which, in accord to CALPHAD calculations with FAB > 0.7, are single-phase BCC structures at T_m and have $T_{use} > 1000$ °C, $E > 100$ GPa, $P <$ \$500/kg and $\rho < 10$ g/cm^3.

Alloy	Database	*FAB*	T_m (°C)	T_{use} (°C)	Phases at 600 °C	ρ (g/cm^3)	*E* (GPa)	*Cost* (\$/kg)
AlCrFeMnMo	PanSol	0.90	1600	1041	Bcc+$AlMo_3$	7.0	213	39
AlCrFeMnV	PanSol	1.00	1528	1133	Bcc	6.0	168	49
AlCrFeMoV	PanSol	1.00	1752	1123	Bcc+$AlMo_3$	6.7	199	79
AlCrFeMoV	PanTi	0.80	1732	1026	Bcc+$AlMo_3$	6.7	199	79
AlCrFeTiV	PanTi	0.90	1937	1023	Bcc+ C14	5.4	150	52
AlCrMnMoTi	PanMo	0.90	1574	1107	Bcc+Mo_3Si+Hcp	6.2	190	42
AlCrMnTiV	PanSol	1.00	1541	1131	Bcc	5.3	149	53
AlCrNbTaV	PanSol	0.90	1729	1021	Bcc+σ+C15	8.5	147	250
AlCrNbVW	PanSol	1.00	2256	1331	Bcc+Bcc	8.9	192	81
AlCrTaTiV	PanTi	1.00	1641	1091	Bcc+ σ	7.6	150	236
AlCuMnMoNb	PanSol	0.70	1912	1083	Bcc+Bcc	7.5	163	83
AlCuMoNbTi	PanTi	0.70	1962	1375	Bcc	6.8	148	86
AlFeMnNbV	PanSol	0.80	1672	1223	Bcc	6.5	134	100
AlFeNbTaV	PanTi	0.70	1656	1036	Bcc	8.7	136	246
AlMnMoNbTi	PanSol	0.80	2019	1351	Bcc	6.6	158	88
AlMnMoNbV	PanSol	0.80	2036	1416	Bcc	7.0	162	120
AlMnNbTiV	PanSol	0.90	1679	1235	Bcc	5.8	119	105
AlMoNbTaV	PanTi	1.00	2202	1520	Bcc	9.1	162	248
CoCrMnMoV	PanSol	0.90	1757	1111	Bcc	8.0	232	77
CoFeMnNbV	PanSol	0.70	1655	1089	Bcc	7.8	163	95
CrCuMoTiV	PanTi	0.70	1999	1239	Bcc	7.3	195	75
CrFeMnMoTi	PanSol	0.90	1683	1002	Bcc+ C14	7.4	223	38
CrFeMoNbV	PanSol	0.90	2023	1034	Bcc+Bcc	8.1	205	112
CrFeMoTiV	PanTi	0.90	1957	1095	Bcc+ C14	7.1	209	75
CrMnMoTiV	PanSol	0.90	1854	1251	Bcc	7.0	206	76
CrMnNbTiV	PanSol	0.90	1567	1136	Bcc+ C14	6.7	156	97
CrMoNbTiV	PanTi	0.90	2146	1458	Bcc	7.3	184	116
CrMoTiWZr	PanNb	0.70	2327	1222	BCC+C15	9.3	220	338
CuFeMnMoV	PanSol	0.80	1716	1152	Bcc+Bcc	8.2	204	70
FeMoNbTiV	PanTi	0.80	1939	1010	Bcc+Bcc+ C14	7.4	173	114
MnMoNbTiV	PanSol	0.80	2103	1434	Bcc	7.4	171	114
MoNbTaTiV	PanTi	1.00	2325	1677	Bcc	9.4	171	238
MoNbTiVZr	PanSol	0.90	2039	1079	Bcc+Bcc	7.1	141	481
MoTiVWZr	PanSol	0.90	2258	1147	Bcc+Bcc+ZrW_2	9.1	197	362

Table 15
6-component equiatomic alloys which, in accord to CALPHAD calculations with FAB > 0.7, are single-phase BCC structures at T_m and have T_{use} > 1000 °C, E > 100 GPa, P < $500/kg and ρ < 10 g/cm^3.

Alloy	Database	*FAB*	T_m (°C)	T_{use} (°C)	Phases at 600 °C	ρ (g/cm^3)	*E* (GPa)	*Cost* ($/kg)
AlCrFeMnNbV	PanSol	0.87	1548	1184	Bcc	6.6	155	86
AlCrMnNbTiV	PanSol	0.93	1533	1171	Bcc	6.0	140	89
AlCrMoNbTiV	PanTi	0.93	1881	1450	Bcc	6.5	164	108
AlCrMoNbVW	PanSol	1.00	1915	1120	Bcc+Bcc	9.1	215	86
AlCuMnMoNbTi	PanSol	0.80	1456	1034	Bcc+Bcc	6.9	154	74
AlCuMoNbTaTi	PanTi	0.73	1843	1420	Bcc	8.6	155	198
AlFeMoNbTaTi	PanTi	0.74	1401	1009	Bcc+ C14	8.5	165	200
AlMnMoNbTiV	PanSol	0.87	1790	1377	Bcc	6.5	154	106
CoCrFeMnMoV	PanSol	0.93	1397	1063	Bcc	8.0	228	65
CoCrFeMoNbV	PanSol	0.87	1578	1018	Bcc+Bcc	8.2	206	100
CrFeMoNbTiV	PanTi	0.80	1585	1037	Bcc+ C14	7.4	188	100
CrFeNbTaTiV	PanTi	0.80	1341	1018	Bcc+ C14	8.7	163	211
CrMoNbTaTiZr	PanTi	0.93	1451	1106	Bcc+C15	8.9	166	435
CrMoNbTiVZr	PanTi	0.87	1428	1088	Bcc+C15	7.1	157	424
CrMoTaTiVZr	PanTi	0.93	1401	1066	Bcc+C15	8.6	172	459

4. Discussion

A screening methodology developed in this work allows us to quickly identify, screen and analyze over one hundred thousand multi principal element alloys at equiatomic compositions for required microstructure and properties. This methodology is based on the automated analysis and application driven screening of thermodynamic and some other properties of the alloys and it can also be applied to non equiatomic alloys. The thermodynamic properties, such as phases present, solidus temperature and maximum use temperature, are determined for each alloy using CAPLPHAD calculations and eight currently available thermodynamic databases developed by CompuTherm LLC (www.computherm.com). Additional properties, such as Young's modulus, density and cost, are calculated from elemental properties using the rule of mixtures. The screening process is facilitated by applying computer programs developed to automate the alloy selection, property calculations and analysis.

4.1. Credibility of CALPHAD calculations

As the present approach is based on the results of CALPHAD calculations, it is important to know levels of credibility of these calculations for every alloy. The available thermodynamic databases include thermodynamic properties of only few ternary alloys, for which complete thermodynamic description of all the binary and ternary systems exists, so that only a few ternary systems can be calculated with full confidence. Since FAT is somewhat FAB dependent (Fig. 1) and since the model parameters for non available ternary systems can be calculated only from existing binary systems, we have given much more weight to the FAB parameter. For the same reason, we excluded all alloys with

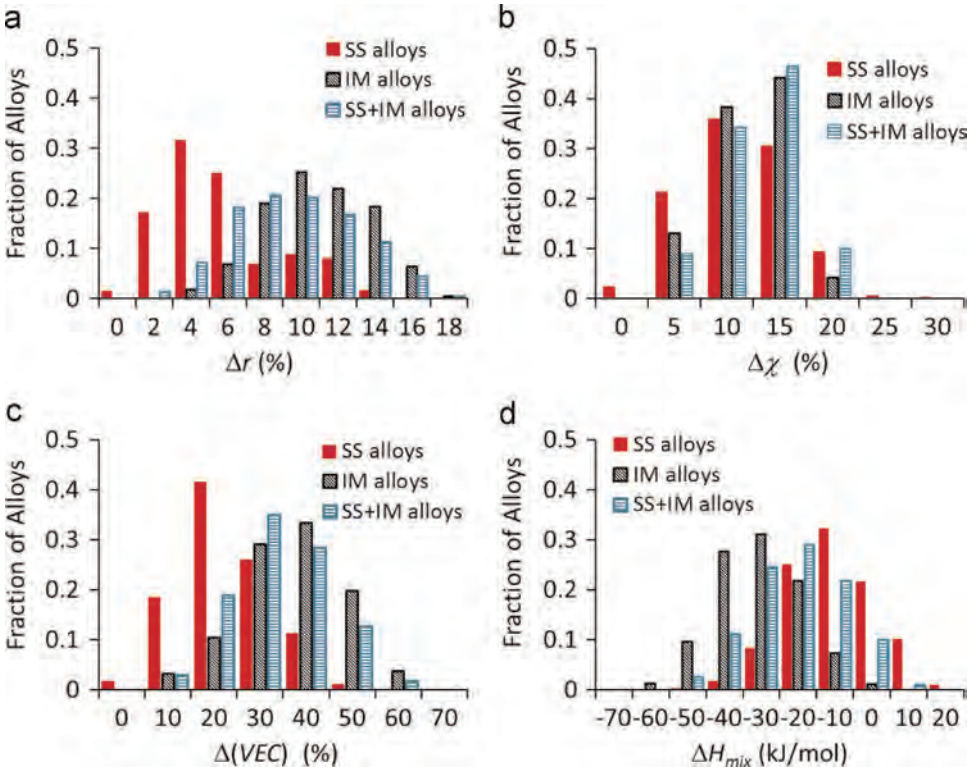

Fig. 10. Distributions of SS, IM and SS+IM equiatomic alloys by (a) the atomic radius difference, (b) electronegativity difference, (c) valence electron concentration difference and (d) enthalpy of mixing of the alloying elements. CALPHAD calculations with FAB > 0.5.

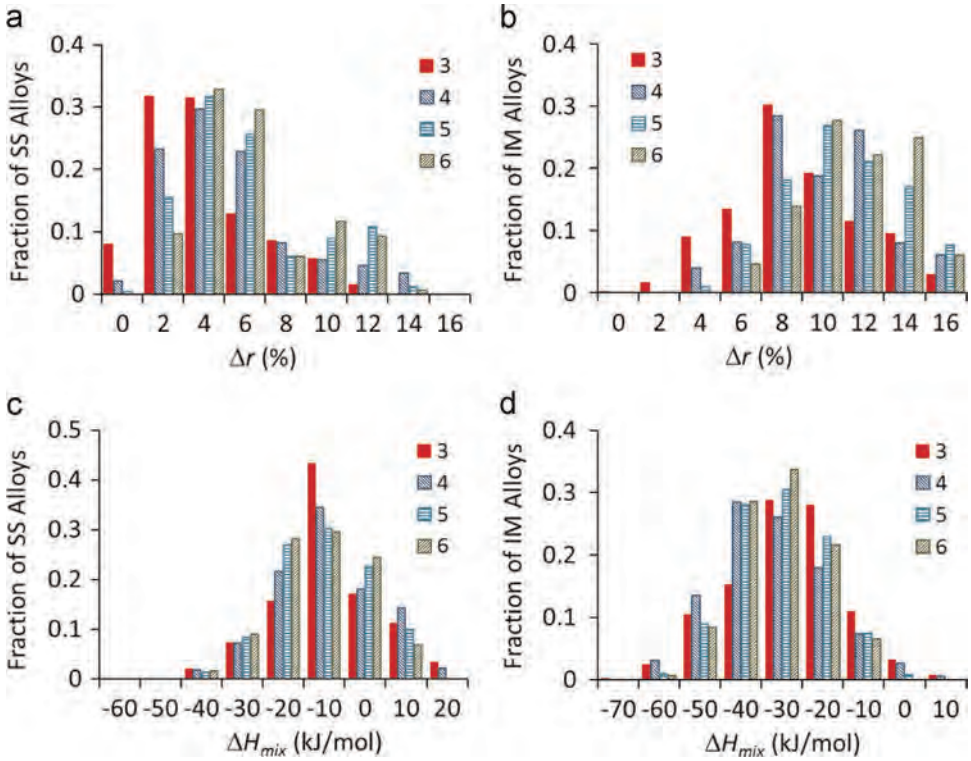

Fig. 11. Distributions of 3, 4, 5 and 6-component (a) SS and (b) IM equiatomic alloys by the enthalpy of mixing of the alloying elements. CALPHAD calculations with FAB > 0.5.

FAB=0 from further analysis. We found that the calculated alloys are almost equally distributed by FAB values and the majority of these alloys have FAT in the range of 0 0.2. We acknowledge that incomplete thermodynamic descriptions may call into question some of the calculated results, and additional experimental ver ifications of the phase compositions of selected alloys are required. Such experimental validations are beyond the scope of a single study, and so the results of calculations are given here (see Tables 6, 9 15) to stimulate future experimental comparisons.

The reported properties distributions by alloy categories are qualitatively similar for alloys with different FAB values, so that the trends reported here for equiatomic alloys with low FAB values are also typical to the smaller number of alloys with higher FAB values. Moreover, the results show that different databases used to cal culate phase diagrams for the same alloy often predict the same phases at T_m and below T_{use}, as well as similar T_m and T_{use} values, if the credibility of the calculations FAB > 0.5. These observations indicate that calculated phase diagrams of a given alloy using different thermodynamic databases, with FAB > 0.5, are also quantitatively consistent. Reasonable agreements are also found between the calculated (with FAB > 0.5) and experimentally re ported phases for over 50 MPEAs (see Supplementary information file).

4.2. Effect of alloy compositions on the formation of disordered SS phases

4.2.1. Effect of the number of alloying elements

The present CALPHAD calculations uncover new trends for equiatomic alloys, some of which contradict current views on high entropy alloy behavior. For example, we show that equiatomic alloys containing only SS phases (SS alloys) dominate over alloys containing only IM phases (IM alloys) at T_m and that the fraction of SS alloys decreases with decreasing temperature (Fig. 3). This re flects the expected competition between entropic terms for solid solutions and formation energies of intermetallics [5,9]. On the other hand, the observation that the fraction of equiatomic SS al loys decreases with an increase in the number of alloying elements seems to contradict the high entropy alloy concept. Assuming, for simplicity, that a competing IM phase is fully ordered and its en tropy of mixing is zero, $(\Delta S_{mix})_{IM} = 0$, a SS phase will be en ergetically favorable if $\Delta H_{IM} > \Delta H_{SS}$ $T\Delta S_{mix}$. Here ΔH_{IM} and ΔH_{SS} are enthalpies of the IM and SS phases measured relative to the enthalpies of pure elements and ΔS_{mix} is the entropy of mixing of elements in a fully disordered SS phase. For equiatomic alloys that are also ideal or regular solutions, $\Delta S_{mix} = \Delta S_{conf} = R \ln(N)$, where R is the gas constant and N is the number of alloying ele ments. For a quasi regular solution, $\Delta S_{mix} = \Delta S_{conf} + \Delta S_{ex}$, where ΔS_{ex} is the excess entropy, which takes into account deviations from random distribution of the alloying elements [49,50]. Be cause ΔS_{ex} is generally small (< 15%) relative to ΔS_{conf} for an equiatomic disordered solution, $\Delta S_{mix} = \Delta S_{conf}$ approximation is used in the following text. Thus, the probability of a SS phase formation during solidification increases with increasing T and N, and a critical temperature, $T_C = (\Delta H_{SS}\ \Delta H_{IM})/\Delta S_{mix}$, exists below which the IM phase is more stable than the SS phase. However, the CALPHAD calculations show that the probability of formation of SS alloys decreases with an increase in N.

There are several issues with the simplified approach above. It is widely appreciated that solid solutions are rarely ideal, and even regular solutions may not be common [31,49]. Further, the ap proach above is only valid if the alloy forms a single solid solution. If two or more solid solutions are formed, then ΔS_{mix} of each SS phase will be less than ΔS_{mix} of the single phase. Finally, a de crease in the fraction of equiatomic SS alloys with an increase in the number of alloying elements can be explained by the com petition between $T\Delta S_{mix}$, which favors random distribution of the alloying elements, and the enthalpies of formation of competing intermetallic phases, which favors elemental ordering. When the number of the alloying elements increases from 3 to 6, $T_m\Delta S_{mix}$

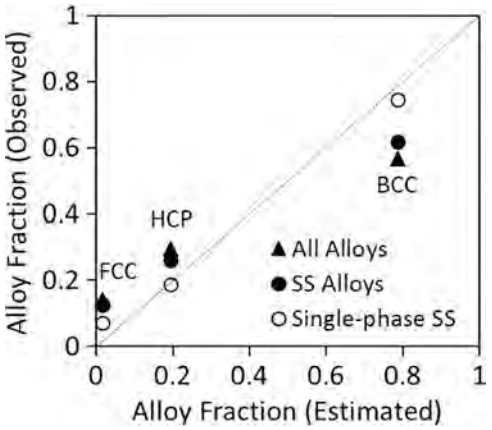

Fig. 12. Relative fractions of equiatomic alloys (all alloys, SS alloys and single-phase SS alloys) containing BCC, HCP and FCC phases, which were estimated from the number of elements with the respective structures (Estimated) and from CALPHAD calculations (Observed). The drawn dotted line corresponds the situation when the observed and estimated values are the same.

increases (in J/mol) from $9.1T_m$ to $14.9T_m$, respectively, or, at $T_m = 1273$ K (1000 °C), from 11.6 kJ/mol to 19.0 kJ/mol. This represents a decrease in entropic energy of the solid solution phase by only 64% when N increases from 3 to 6. At the same time, the number of the binary and ternary systems included in an alloy increase from 3 and 1 for a 3 component alloy to 15 and 20 for a 6 component alloy. Therefore, the number of possible intermetallic phases increases dramatically with increasing N, increasing the probability that one of these intermetallic phases may have the Gibbs free energy more negative than that of the SS phase. Indeed, the enthalpies of mixing of IM alloys are, in average, 10–30 kJ/mol more negative than those of SS alloys and the difference increases with an increase in the number of components (see Figs. 10d and 11). Further, classical considerations suggest that formation enthalpies for intermetallic phases are even more negative than the enthalpy of mixing for the same alloy. This analysis shows that the probability of forming an intermetallic phase with $\Delta H_{IM} < \Delta H_{SS} - T_m\Delta S_{mix}$ should increase with increasing N. This also explains a rapid increase in the fraction of multi phase (SS+IM) alloys containing both SS and IM phases with an increase in N. Finally, there is also a general trend for ΔS_{mix} to fall below $R\ln(N)$ with a decrease in temperature. A consequence of deviations from the completely random alloy, this reflects local ordering or clustering and favors the formation of IM over SS phases.

We also show that at T_m, the majority of SS equiatomic alloys contain 1 or two phases, and only a few contain three phases. The number of phases in IM equiatomic alloys correspond to the first, second and third largest number of phases (see Fig. 5). For example, 4 component IM alloys contain 2, 3 or 4 phases, and 6 component IM alloys contain 4, 5 or 6 phases. (SS+IM) alloys contain ≥ 2 phases. The CALPHAD results predict a majority of the single phase 3 component alloys and all single phase 4, 5 and 6 component alloys as SS alloys. The trend is consistent with an increasing entropic contribution with increasing number of components. When two or more SS phases form during solidification, ΔS_{mix} generally decreases because of the compositions of these phases deviate from the equiatomic composition, and formation of IM phases becomes easier. Thus an alternative explanation is the increasing instability. This explains why SS+IM alloys dominate among the multi phase alloys.

4.2.2. Distributions of SS phases by their crystal structures

BCC and HCP are the most common phases in the calculated equiatomic alloys and the FCC SS phase is the fifth most common, which is preceded by two intermetallic phases, M_5Si_3 ($D8_8$) and B2. The high fraction of alloys containing silicide phases (M_5Si_3, M_5Si_4, and M_3Si_2) is probably due to very negative, often below 50 kJ/mol [51–53] enthalpies of formation of these phases. Because of this, every Si containing equiatomic alloy contains silicides. The B2 phase requires ordering of elements on two interpenetrating simple cubic sub-lattices. In binary systems, this phase is present at equiatomic compositions and often has a large solubility range [54]. In ternary and higher order equiatomic alloys containing B2 forming binaries, the large solubility range of the alloying elements increases the entropic term of this phase, which, together with high negative enthalpies of formation, noticeably reduces the Gibbs free energy of B2 and favors formation of this phase.

The observed relative distribution of equiatomic alloys containing disordered BCC, HCP and FCC phases can be correlated with the number of elements having these respective crystal structures, which were used to produce the processed equiatomic alloys. Of the 27 elements in this work, 15 have the BCC crystal structure (Cr, Dy, Fe, Gd, Hf, Mn, Mo, Nb, Sc, Ta, Ti, V, W, Y, Zr), 13 have an HCP structure (Co, Dy, Hf, Lu, Mg, Re, Ru, Ti, Zr, Sc, Gd, Tm, Y), 8 elements (Ag, Al, Co, Cu, Fe, Mn, Ni, Rh) have the FCC structure and one element (Si) has a diamond cubic crystal structure. 10 elements (Co, Dy, Fe, Gd, Hf, Mn, Sc, Y, Zr) are allotropes with different crystal structures at different temperatures. Assuming that BCC, HCP and FCC phases predominantly form in equiatomic alloys consisting of the elements with the same crystal structures, the relative fractions of these alloys are estimated to be 79%, 19% and 2%, respectively. Fig. 12 compares the estimated fractions of the alloys containing BCC, HCP and FCC phases with the respective relative fractions, in accord to CALPHAD calculations, of (a) all calculated alloys, (b) SS alloys and (c) single phase SS alloys containing these phases. The comparison shows similar trends of the estimated and observed (CALPHAD calculated) values. Moreover, the observed fractions of BCC, HCP and FCC single phase SS alloys are almost the same as the respective estimated alloy fractions. This result may indicate that the Hume–Rothery rule that requires the same crystal structure of the elements to form extended solid solutions may also apply to solid solution phases formed in equiatomic alloys.

The elements that likely promote the formation of SS phases in the present equiatomic alloys are Cr, Mn, Mo, Nb, Re, Rh, Ru, Ta, Ti, V and W. Seven of these (Cr, Mn, Mo, Nb, Ta, V and W) have a BCC crystal structure, two (Mn, Rh) have an FCC crystal structure and three (Re, Ru, Ti) have an HCP crystal structure. Additional studies are required to understand why these elements are more preferable in the SS phases.

4.3. The solidus and maximum use temperatures of equiatomic alloys

An important finding from this work is that the fractions of calculated equiatomic alloys with solidus temperature and maximum use temperature above 1000 °C decrease considerably with an increase in the number of alloying elements (Fig. 7). For example, 42% of 3 component alloys and only 11% of 6 component alloys have $T_m \geq 1400$ °C; 7% of 3 component alloys and only 0.5% of 6 component alloys have $T_{use} \geq 1400$ °C. This indicates that an increase in the number of alloying elements in equiatomic alloys reduces the temperature range of potential use of these alloys and makes them less attractive for high temperature applications. Nevertheless, in the present work we uncover a large number of potential high temperature alloy systems, including 1,455 single phase SS alloys, with $T_{use} > 1000$ °C. Further, Tables 9–15 list 157 new multi phase alloys that may be age hardened for improved high temperature strength and are thus candidate alloy bases for future studies.

4.4. Density, Young's modulus and cost of equiatomic alloys

The density, Young's modulus and cost of the calculated equiatomic alloys vary from 2.37 g/cm^3 to 18 g/cm^3, 54 GPa to 439 GPa, and \$3/kg to over \$100,000/kg, respectively. With an increase in the number of the alloying elements, the extreme va lues move towards the average values and the ranges of properties become narrower. Such behavior is expected as the mixture of more elements results in stronger averaging their properties.

4.5. Potential equiatomic alloys for high temperature structural applications

Good ductility and fracture toughness generally involve a solid solution (SS) primary phase, while potent strengthening me chanisms (e.g. SS and precipitation strengthening) may require a second (SS or IM) phase that can be dissolved above T_{use} but below the solidus, T_m, and can be re precipitated below T_{use}. High tem perature structural applications require alloys with $T_{use} > 1000$ °C. To meet these conditions, 1455 equiatomic alloys with a single SS phase at T_m and no phase transformations below 1000 °C have been identified, and compositions of some of these alloys are given in Table 9 through Table 15. The number of alloys has been further down selected by restricting their Young's modulus to above 100 GPa, density below 10 g/cm^3, and cost below \$500 per kilo gram. Only 278 of the calculated equiatomic alloys pass these criteria, among which 272 are BCC and only 6 are FCC structures at T_m. None of the HCP equiatomic alloys have the combination of properties, mainly because of high cost. Many of the selected al loys have two or three phases below T_{use}, with a solid solution as a major phase. The existence of two or three phases below T_{use} in dicates that the secondary phases can be dissolved at tempera tures between T_{use} and T_m, and thus these alloys can be heat treatable.

4.6. Refined Hume Rothery rules and phenomenological criteria for SS phase formation in equiatomic alloys

Hume Rothery rules well describe solid solution phase forma tion in MPEAs. If an MPEA satisfies all four rules, the present CALPHAD predictions show it to have a SS structure, at least at T_m. However, these rules are not definitive, as there are considerable numbers of SS MPEAs that do not follow these rules. For example, the electronegativity difference between alloying elements can be as high as 30% and valence electron concentration differences are as high as 55% in some SS forming MPEAs (Fig. 10). As discussed above, SS MPEAs do not require the same crystal structure of al loying elements and many SS MPEAs contain elements with dif ferent crystal structures. Two examples are an FCC CoFeNiTmV alloy, consisting of 3 elements with FFC structures, one element with HCP structure and one element with BCC structure (Table 9), and a BCC AlCuMoNbTaTi, consisting of two elements with FCC structure and four elements with BCC structure (Table 15). There are also many already reported alloys consisting of elements with different crystal structures [5,11]. Only one Hume Rothery rule, namely atomic radius difference, seems to work well for all MPEAs. Indeed, among tens of thousands of calculated equiatomic MPEAs, all SS MPEAs have $\Delta r < 15\%$ and the frequency of SS MPEAs in creases with decreasing Δr (Fig. 10). We conclude that in equia tomic MPEAs atomic size has a much stronger influence on for mation of SS phases than chemical interactions (electronegativity, enthalpy of mixing) between the elements. This conclusion is also supported by the weak dependence of the types of phases on the enthalpy of mixing of alloying elements. Although ΔH_{mix} of IM MPEAs is, on average, more negative than that of SS MPEAs, a majority of both types of alloys have similar ΔH_{mix} values. It is likely that the enthalpy of formation of intermetallic phases, ΔH_f, rather than ΔH_{mix}, as discussed in previous sections, controls phase formations in MPEAs.

5. Conclusions

An approach for the computational analysis and screening of over one hundred thousand equiatomic alloys for high tempera ture structural applications has been developed. The numbers and types of phases, reaction temperatures, and some physical prop erties of 3 to 6 element equiatomic alloys have been analyzed using this approach. The calculated alloys have been divided into three categories: solid solution (SS) alloys that contain disordered solid solution phases only, intermetallic (IM) alloys that contain intermetallic and/or ordered solid solution phases only, and (SS+IM) alloys that contain both SS and IM phases. The following conclusions have been made.

1. The fractions of SS and IM alloys decrease and the fraction of (SS+IM) alloys increases with an increase in the number of alloying elements from 3 to 6.
2. Almost all single phase equiatomic alloys are SS alloys. Ac counting for the existence of multi phase SS alloys, the fraction of SS alloys decreases with an increase in the number of phases in the alloys.
3. The fraction of IM equiatomic alloys increases with an increase in the number of phases. Not surprisingly, there are no single phase IM alloys containing 4 to 6 components. 5 component IM alloys contain 3, 4 or 5 phases, and 6 component IM alloys contain 4, 5 or 6 phases.
4. The majority of equiatomic alloys containing two or more phases are (SS+IM) alloys.
5. BCC, HCP and FCC SS phases, three silicide phases (M_5Si_3, M_5Si_4 and M_3Si_2), B2, and two Laves phases are the most common phases among 453 unique phases identified in the calculated alloys.
6. The maximum use temperature decreases considerably with an increase in the number of alloying elements.
7. An increase in the number of alloying elements considerably reduces the range of properties, such as density, elastic mod ulus and cost. The highest and lowest values of properties move toward the average values. Thus an increase in the number of alloying elements in equiatomic alloys considerably reduces the opportunity to meet extreme properties requirements.
8. Here we list 157 new equiatomic alloys that are single phase SS at T_m. Some of these alloys may be age hardened for improved strength, providing new alloy bases for future development studies.

Acknowledgments

Technical help from Mr. Adam Shiveley (AFRL) in writing a computer script for automated, continuous running of multiple Pandat batch files and numerous discussions with Dr. Fan Zhang (CompuTherm LLC) are greatly appreciated. This work was con ducted at the Air Force Research Laboratory, Materials and Man ufacturing Directorate. Work by ONS was supported through the AF on site Contract FA8650 10 5226 managed by UES, Inc., Day ton, Ohio.

Appendix A. Supplementary material

Supplementary data associated with this article can be found in

the online version at http://dx.doi.org/10.1016/j.calphad.2015.04.009.

References

[1] M.J. Donachie, S.J. Donachie, Superalloys: A Technical Guide, Materials Park, OH, 2nd ed., ASM International, 2002.
[2] T.M. Pollock, A. Tin, J. Propuls. Power 22 (2006) 361–374.
[3] P. Tsakiropoulos, Beyond Nickel Based Superalloys, in: R. Blockley, Wei Shyy (Eds.), Encyclopedia of Aerospace Engineering, John Wiley & Sons Ltd, Chichester, UK, 2010, pp. 2345–2354.
[4] J.-W. Yeh, S.-K. Chen, S.-J. Lin, J.-Y. Gan, T.-S. Chin, T.-T. Shun, C.-H. Tsau, S.-Y. Chang, Adv. Eng. Mater. 6 (2004) 299–303.
[5] B.S. Murty, J.-W. Yeh, S. Ranganathan, High Entropy Alloys, Butterworth-Heinemann, London, UK, 2014.
[6] B. Cantor, I.T.H. Chang, P. Knight, A.J.B. Vincent, Mater. Sci. Eng. A 375–377 (2004) 213–218.
[7] D.B. Miracle, J.D. Miller, O.N. Senkov, C. Woodward, M.D. Uchic, J. Tiley, Entropy 16 (2014) 494–525.
[8] O.N. Senkov, J.W. Miller, D.B. Miracle, C. Woodward, Nat. Commun. 6 (2015) 6529.
[9] M.-H. Tsai, J.-W. Yeh, Mater. Res. Lett. 2 (2014) 107–123.
[10] J.W. Yeh, Ann. Chim.-Sci. Mater. 31 (2006) 633–648.
[11] Y. Zhang, T.T. Zuo, Z. Tang, M.C. Gao, K.A. Dahmen, P.K. Liaw, Z.P. Lu, Prog. Mater. Sci. 61 (2014) 1–93.
[12] J.W. Yeh, Y.L. Chen, S.J. Lin, S.K. Chen, in: H.B. Ramirez, J.G. CabanasMoreno, H. A. CalderonBenavides, K. Ishizaki, A. SalinasRodriguez (Eds.), High-entropy Alloys—a new era of exploitation, Advanced Structural Materials III, 2007, pp. 1–9.
[13] R. Kozak, A. Sologubenko, W. Steurer, Z. Kristallogr.-Cryst. Mater. 230 (2015) 55–68.
[14] B. Cantor, Entropy 16 (2014) 4749–4768.
[15] O.N. Senkov, C. Woodward, D.B. Miracle, JOM. 66 (2014) 2030–2042.
[16] O.N. Senkov, G.B. Wilks, D.B. Miracle, C.P. Chuang, P.K. Liaw, Intermetallics 18 (2010) 1758–1765.
[17] K.B. Zhang, Z.Y. Fu, J.Y. Zhang, J. Shi, W.M. Wang, H. Wang, Y.C. Wang, Q. J. Zhang, J. Alloys Compd. 502 (2010) 295–299.
[18] K.B. Zhang, Z.Y. Fu, Intermetallics 22 (2012) 24–32.
[19] J. Li, Y. Lu, Y. Dong, T. Wang, Z. Cao, T. Li, Intermetallics 44 (2014) 37–43.
[20] W.H. Liu, Y. Wu, J.Y. He, Y. Zhang, C.T. Liu, Z.P. Lu, JOM 66 (2014) 1973–1983.
[21] F. Otto, Y. Yang, H. Bei, E.P. George, Acta Mater. 61 (2013) 2628–2638.
[22] K.Y. Tsai, M.H. Tsai, J.W. Yeh, Acta Mater. 61 (2013) 4887–4897.
[23] M.G. Poletti, L. Battezzati, Acta Mater. 75 (2014) 297–306.
[24] Z. Wang, Y. Huang, Y. Yang, J. Wang, C.T. Liu, Scr. Mater. 94 (2014) 28–31.
[25] S. Guo, C. Ng, J. Lu, C.T. Liu, J. Appl. Phys. 109 (2011).
[26] N.D. Stepanov, D.G. Shaysultanov, G.A. Salishchev, M.A. Tikhonovsky, E. E. Oleynik, A.S. Tortika, O.N. Senkov, J. Alloys Compd. 628 (2015) 170–185.
[27] Z.S. Nong, J.C. Zhu, Y. Cao, X.W. Yang, Z.H. Lai, Y. Liu, Mater. Sci. Technol. (UK) 30 (2014) 363–369.
[28] X. Yang, Y. Zhang, Mater. Chem. Phys. 132 (2012) 233–238.
[29] A. Takeuchi, A. Inoue, Mater. Trans.—Jpn. Inst. Met. 46 (2005) 2817–2829.
[30] Y.A. Chang, H.B. Cao, S.L. Chen, F. Zhang, Y. Yang, W.S. Cao, K.S. Wu, Phase equilibria, in: S.L.S.D.U. Furrer (Ed.), ASM Handbook on Fundamentals of Modeling for Metals Processing, ASM International Materials Park, OH, USA, 2009, pp. 443–457.
[31] F. Zhang, C. Zhang, S.L. Chen, J. Zhu, W.S. Cao, U.R. Kattner, Calphad: Comput. Coupling Phase Diag. Thermochem. 45 (2014) 1–10.
[32] C. Zhang, F. Zhang, S. Chen, W. Cao, JOM 64 (2012) 839–845.
[33] Y.A. Chang, S.L. Chen, F. Zhang, X.Y. Yan, F.Y. Xie, R. Schmid-Fetzer, W.A. Oates, Prog. Mater. Sci. 49 (2004) 313–345.
[34] U.R. Kattner, JOM 49 (1997) 14–19.
[35] K.C. Chou, Y.A. Chang, Ber Bunsenges., Phys. Chem. 93 (1989) 735–741.
[36] F.J. Wang, Y. Zhang, H.A. Davies, G.L. Chen, J. Eng. Mater. Technol. 191 (2009) 034501.
[37] H.-P. Chou, Y.-S. Chang, S.-K. Chen, J.-W. Yeh, Mater. Sci. Eng. B 163 (2009) 184–189.
[38] Y.J. Zhou, Y. Zhang, Y.L. Wang, G.L. Chen, Appl. Phys. Lett. 90 (2007) 181904.
[39] J.W. Qiao, S.G. Ma, E.W. Huang, C.P. Chuang, P.K. Liaw, Y. Zhang, Mater. Sci. Forum 688 (2011) 419–425.
[40] Y. Zhang, S.G. Ma, J.W. Qiao, Metall. Mater. Trans. A 43 (2012) 2625–2630.
[41] C. Li, J.C. Li, M. Zhao, Q. Jiang, J. Alloys Compd. 475 (2009) 752–757.
[42] H. Cui, L. Zheng, J. Wang, Appl. Mech. Mater. 66–68 (2011) 146–149.
[43] P.P. Bhattacharjee, G.D. Sathiaraj, M. Zaid, J.R. Gatti, C. Lee, C.-W. Tsai, J.-W. Yeh, J. Alloys Compd. 587 (2014) 544–552.
[44] T.-T. Shun, L.-Y. Chang, M.-H. Shiu, Mater. Sci. Eng. A 556 (2012) 170–174.
[45] S. Varalakshmi, M. Kamaraj, B.S. Murty, Metall. Mater. Trans. A 41 (2010) 2703–2709.
[46] W. Hume-Rothery, R.W. Smallman, C.W. Haworth, The Structure of Metals and Alloys, The Institute of Metals, London, 1969.
[47] Y.X. Zhuang, W.J. Liu, Z.Y. Chen, H.D. Xue, J.C. He, Mater. Sci. Eng. A 556 (2012) 395–399.
[48] Y. Zhang, Y.J. Zhou, J.P. Lin, G.L. Chen, P.K. Liaw, Adv. Eng. Mater. 10 (2008) 534–538.
[49] J. Ganguly, EMU Notes in Mineralogy, (2001) 37–69.
[50] W.A. Oates, J. Phase Equilib. Diffus. 28 (2007) 79–89.
[51] S.V. Meschel, O.J. Kleppa, J. Alloys Compd. 280 (1998) 231–239.
[52] S.V. Meschel, O.J. Kleppa, J. Alloys Compd. 274 (1998) 193–200.
[53] S.V. Meschel, O.J. Kleppa, J. Alloys Compd. 267 (1998) 128–135.
[54] J.P. Neumann, Y.A. Chang, H. Ipser, Scr. Mater. 10 (1976) 917–922.